Improving the Steering Law Throughput Calculation by Defining Effective Parameters for 3D Virtual Environments

Mohammadreza Amini
Department of Computer Science & Software Engineering
Concordia University
Montreal, Quebec, Canada
mohammadreza.amini@concordia.ca

Wolfgang Stuerzlinger
School of Interactive Arts + Technology (SIAT)
Simon Fraser University
Vancouver, British Columbia, Canada
w.s@sfu.ca

Shota Yamanaka
LY Corporation
Tokyo, Japan
syamanak@lycorp.co.jp

Hai-Ning Liang
Computational Media and Arts Thrust
The Hong Kong University of Science and Technology (Guangzhou)
Guangzhou, Guangdong, China
hainingliang@hkust-gz.edu.cn

Anil Ufuk Batmaz
Department of Computer Science & Software Engineering
Concordia University
Montreal, Quebec, Canada
ufuk.batmaz@concordia.ca

Abstract

Throughput is a widely used performance metric, combining speed and accuracy into a single measure, while reducing the effect of subjective speed–accuracy trade-offs. Despite its wide application in 2D steering tasks, its direct extension to 3D presents unique challenges since 3D trajectories exhibit higher variability, and perceptual–motor factors undermine existing formulations. Consequently, throughput has not been systematically adopted for evaluating steering in 3D virtual environments. In this paper, using a controlled virtual reality user study with a ring-and-wire task, we introduce and validate a novel throughput formulation for 3D steering based on the bivariate standard deviation of the trajectory for the effective width calculation. Our results show that this formulation provides smoother throughput values across subjective speed–accuracy differences and improves model fit compared to traditional approaches. This work advances our theoretical understanding of the Steering law in 3D contexts, provides researchers and practitioners with a robust evaluation method, and establishes a foundation for future studies of complex 3D trajectory interactions.

CCS Concepts

• **Human-centered computing** → **User models**; **HCI theory, concepts and models**; **Virtual reality**.

Keywords

Steering Law, Virtual Reality, Trajectory-based Interactions, Behavior Modeling, Throughput.

ACM Reference Format:
Mohammadreza Amini, Wolfgang Stuerzlinger, Shota Yamanaka, Hai-Ning Liang, and Anil Ufuk Batmaz. 2026. Improving the Steering Law Throughput Calculation by Defining Effective Parameters for 3D Virtual Environments.

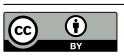

CHI '26, Barcelona, Spain

ACM ISBN 979-8-4007-2278-3/26/04
https://doi.org/10.1145/3772318.3790579

In *Proceedings of the 2026 CHI Conference on Human Factors in Computing Systems (CHI '26), April 13–17, 2026, Barcelona, Spain.* ACM, New York, NY, USA, 20 pages. https://doi.org/10.1145/3772318.3790579

1 Introduction

Steering is a fundamental task in Human–Computer Interaction (HCI), appearing in 2D desktop applications and 3D immersive environments [2, 128]. It involves *"the continuous movement through a constrained path"*, such as navigating through nested menus, drawing curves, shape tracing, or manipulating scrollbars [2, 147]. Studying steering performance is a core aspect of HCI research [2, 25], helping us to design user interfaces [11, 66, 113], evaluate and compare interaction techniques [3, 66], and better understand human motor behavior.

Researchers have developed mathematical models that reliably describe the complexity of human motor behaviors in specific tasks [147]. For pointing, Fitts' law is a widely used model that serves as a foundation for the design and evaluation of user interfaces, interaction techniques, and input devices [8, 84]. It predicts the Movement Time (*MT*) using task difficulty, i.e., the Index of Difficulty (*ID*). Inspired by Fitts' law, Accot and Zhai [2] later proposed the Steering law to model *MT* in steering tasks, which is also a widely used model of human motor behavior in HCI [129, 140, 147].

Throughput is a broadly used metric in Fitts' law studies [8, 18, 87], combining speed and accuracy into one measure, reflecting the trade-off that greater accuracy demands more time [27, 86–88]. It is recognized in ISO 9241-411 as an evaluation tool for input devices [61], and is used as a performance metric for comparing interaction techniques and user groups [8, 18, 66, 84]. Recent work has also shown that throughput describes 2D steering task performance better [66, 67].

Prior work has shown that throughput calculated with *nominal* parameters can be unstable across different subjective speed-accuracy biases. To address this, researchers proposed using *effective* Width (W_e) and Amplitude (A_e), which better describe *users' actual behaviors* [87, 95, 148]. Early work indicated that the *effective throughput* smooths the effect of varying speed-accuracy strategies for pointing [87]. Through a study of a 2D steering task, Kasahara

et al. [66] empirically demonstrated the effectiveness of throughput as a performance metric for steering, showing that effective parameters substantially stabilize throughput and improve the Steering law model-fit across speed–accuracy biases [66].

Extending 2D findings, researchers have explored the Steering law in 3D environments. For example, Liu et al. [78] empirically demonstrated that the Steering law holds in 3D environments, showing a linear relationship between path length, width, and MT. Other works have extended the model to account for 3D-specific factors, such as directional movements [129], frame rate [128], and curvatures [60, 80]. Despite this growth, the effectiveness of throughput as a performance metric in 3D settings remains uninvestigated.

Direct transfer from 2D work to 3D presents challenges, such as the effect of visual depth cues [15, 21], the absence of physical support [128], and the added degrees of freedom [78, 128], all of which can increase movement variability. Moreover, even in 2D, as Kasahara et al. [66] highlighted, the theoretical justification for using effective parameters to stabilize throughput remains limited. Thus, there is a need to examine whether effective parameters offer a reliable method for throughput calculation in 3D steering tasks, and to adapt the metric to the unique characteristics of 3D interactions.

In this paper, we conducted a user study in VR with multiple steering orientations. The study examined 3D mid-air interaction under different subjective speed–accuracy biases, i.e., emphasizing speed or accuracy, and a neutral condition. The primary motivation behind this work is to strengthen the methodological foundation for evaluating performance in 3D steering tasks. In short, our main contributions include:

(1) We demonstrate that throughput is a valid performance metric for 3D steering tasks in VR;
(2) We show that using bivariate effective width ($W_{e,bi}$) and amplitude (A_e) makes throughput less variant across subjective speed–accuracy biases than existing alternatives; and
(3) We provide a refined, empirically validated throughput calculation method for 3D steering, outlining its implications for future methodology and interaction technique design.

2 Related Work

2.1 Steering law

The Steering law is a human motor behavior model capturing steering performance using a mathematical formulation that describes *MT* based on the spatial properties of a constrained path (see Equation 1). Accot and Zhai [2] introduced the Steering law by extending the principles of Fitts' law [38], a widely-studied model of pointing performance in both 2D [24, 84, 85, 143] and 3D [8, 18, 118, 127]. They showed that Fitts' law also applies to goal-crossing tasks, and conceptualized steering as a continuous sequence of such crossings. By dividing the path C into infinitesimal segments dx, they derived *MT* by integrating the inverse of the path thickness $W(x)$ at any given point (x) along the trajectory (see Equation 1). Accot and Zhai further showed that for linear paths with a constant Width of W and Amplitude of A, the model can be simplified Equation 2. The ratio of path length A to width W in Equation 2 defines the steering task's nominal Index of Difficulty (ID_n).

$$MT = a + b \int_C \frac{dx}{W(x)} \tag{1}$$

$$MT = a + b \cdot ID_n, ID_n = \frac{A}{W} \tag{2}$$

The Steering law has served as a framework for evaluating interaction techniques [4, 76, 138], input devices [3, 110], and user groups [104, 149, 151]. It has been used for designing and optimizing user interfaces [5, 6, 11, 113]. Follow-up studies have refined the model to deepen understanding of human steering behavior while accounting for, e.g., the latency [138] or Control-Display (C-D) ratio [4], and for more complex scenarios, e.g., steering through corners [97], within successive objects [140], and along narrowing or widening tunnels [135]. These examples highlight the growing importance of the Steering law in HCI, supporting both theory and practice.

With advancements in 3D interactions, the Steering law has been increasingly applied across diverse 3D contexts, from direct object manipulation [9, 68, 80, 92, 128, 129] to locomotion tasks [90, 91, 141], like virtual driving [141, 147] and drone piloting [60]. In early attempts, researchers explored the Steering law for navigating through 3D space [99]. Later, Liu et al. [78] proposed refined models of the Steering law, accounting for path curvature and 3D orientation, and empirically demonstrated the validity of the Steering law in 3D manipulation tasks.

The Steering law was also investigated in immersive VR Head-Mounted Displays (HMDs) [117, 141, 145]. Wei et al. explored and modeled steering behavior in VR, and showed that movement direction significantly affected movement time and average speed [129]. Wei et al. [128] also explored other factors affecting steering performance, including frame rate, path features, and curvature, and proposed refined Steering law models with improved predictive accuracy. Recently, Amini et al. [9] compared two common 3D steering tasks (Ring-and-Wire and Ball-and-Tunnel), highlighting how task design influences steering performance.

2.2 Throughput and Effective Calculation

As users attempt faster movements, i.e., *MT* decreases, their performance becomes more erratic, reflecting the well-known speed–accuracy trade-off, widely studied in pointing tasks [18, 49, 87, 93, 134]. To capture both aspects in a single measure, HCI studies commonly use Throughput [8, 18, 66]. Throughput is standardized with ISO 9241-411 as a performance metric for evaluating input devices with pointing tasks. It is defined as the ratio of task difficulty (*ID*) to Movement Time (*MT*) (see Equation 3), based on the empirical finding that *MT* increases with *ID*.

$$TP = \frac{ID}{MT} \tag{3}$$

$$W_e = 4.133 \cdot \sigma_x \tag{4}$$

$$ID_{e,\,\text{pointing}} = \log_2\left(\frac{A_e}{W_e} + 1\right) \tag{5}$$

Subjective speed-accuracy biases are an inevitable implicit factor in HCI studies [27, 66, 142]. Such biases can also be shaped by task framing, where instructions are given to emphasize speed, accuracy, or a balance of both [40, 50, 87]. These instructional conditions have

been recognized as a key factor affecting movement behavior and motor performance [83, 94, 96].

Rather than nominal values, previous work has advocated using effective parameters in throughput, which better capture actual user behaviors [27, 66, 87]. In pointing tasks, effective parameters are typically derived from the standard deviation of selection endpoints (σ_x in Equation 4) for the effective width, and from the mean traversed distance for A_e, together forming the effective *ID* (see Equation 5) [18, 87]. This approach is recommended by ISO 9241-411 for calculating throughput [61].

As prior work noted [18, 66, 87], throughput should *ideally* be invariant to subjective speed–accuracy biases so that performance reflects the system's underlying capability rather than the temporary strategies adopted by users, which is important for HCI researchers and practitioners using throughput as a performance metric combining speed and accuracy [8, 67, 84].

MacKenzie and Isokoski demonstrated that effective throughput remains invariant under systematically introduced biases [87]. In their study, the authors controlled the speed-accuracy bias through the MT [87]. Later, by replicating MacKenzie and Isokoski's study under a broader range of speed–accuracy strategies, Olafsdottir et al. [95] challenged MacKenzie and Isokoski's invariance claim [87], and reported that their throughput calculation was not stable but changed significantly as task instructions shifted from emphasizing speed to accuracy.

Kasahara et al. [67] examined the applicability of throughput in 2D goal-crossing, showing that effective parameters help stabilize values. Kasahara et al. [66] extended these findings to steering, showing that using the effective width W_e (see Equation 6, where σ_x denotes trajectory spread perpendicular to movement direction) yields smoother throughput values. They also showed that incorporating A_e (the average steered distance) reduces throughput variance in 2D steering for higher movement variability, e.g., in circular paths.

$$ID_{e,\,\text{steering}} = \frac{A_e}{W_e} = \frac{A_e}{4.133 \cdot \sigma_x} \tag{6}$$

Still, the majority of studies of throughput focus on the 2D context or 3D selection tasks. In 3D environments, Batmaz and Stuerzlinger investigated mid-air pointing tasks in VR [18]. They found that effective throughput is not invariant to different task execution strategies and highlighted that the speed–accuracy trade-off becomes harder to predict with the additional perceptual and motor demands of 3D [18]. However, to the best of our knowledge, no studies have systematically *investigated the effectiveness of throughput in 3D steering scenarios nor proposed an empirically validated method for its calculation*, accounting for subjective speed-accuracy biases.

Addressing this gap is essential as researchers and practitioners continue to use it in both pointing and steering. Rather than using separate metrics like *MT* and error rate, investigating effective throughput gains importance as its ability to provide a holistic measure of motor performance by integrating speed and accuracy [18, 66, 84], its relative independence from task difficulty, i.e., *ID* [66, 134], and its widespread acceptance as a standard for comparing devices [85, 108, 117], interaction techniques [16, 20, 102], and user groups [109, 131, 133] across both 2D [84, 95] and 3D [8, 18] environments.

Moreover, insights from 2D scenarios cannot be directly transferred to 3D cases, as motor performance in 3D introduces its own distinct challenges. On the perceptual side, HMDs can alter spatial judgments by introducing depth-related conflicts, e.g., the Vergence–Accommodation Conflict (VAC) [15, 58], stereo deficiencies [17, 56], and diplopia [23]. Motor tasks in VR often require extended arm movements or mid-air interaction, introducing fatigue [57, 62, 124], tremor [28, 73], or inaccuracies stemming from limitations in hand tracking systems [1, 51, 98, 103], and often lack tactile feedback [55, 74, 117]. These combined challenges imply that the speed–accuracy relationship in VR does not necessarily mirror that of 2D contexts. Few studies [18, 65] have systematically examined how users adjust performance when prioritizing speed or accuracy in 3D contexts. Compared to discrete selection, continuous motions such as 3D steering show a unique speed-accuracy trade-off. Unlike pointing, steering requires sustained control along a constrained path, where small deviations can lead to cumulative errors or failure. Also, in 3D steering, the cost of overshooting or deviation is higher due to compounded perceptual-motor limitations [9, 15, 17]. Further, the absence of physical support [20, 116], restricted peripheral vision [13, 69, 72], increased cognitive load [107, 123], and ambiguous visual cues [7, 14, 44] can all amplify the influence of users' confidence and chosen strategies [18].

In this work, we propose a calculation method that is experimentally validated and tailored to the unique characteristics of 3D steering. This is important as it enhances the utility and reliability of throughput by enabling fairer comparisons across subjective biases [66], improving result comparability across studies [18], and providing a more robust basis for evaluation for both researchers and practitioners. Our ultimate goal is to establish a comprehensive foundation that not only advances current evaluation practices but also guides future research on the speed–accuracy trade-off in 3D steering interaction.

3 Defining Effective Parameters in 3D

In pointing tasks, the effective width is defined via Equation 4, where σ_x is the univariate standard deviation of selection endpoints projected onto the axis collinear to movement (x), aligning with the one-dimensional nature of Fitts' law [18, 84, 87]. The 4.133 factor is derived from the entropy of a normal distribution ($\log_2\left(\sqrt{2\pi e} \times \sigma\right)$), and corresponds to the span of ±2.066 standard deviations of the unit-normal curve, which encloses 96% of the distribution [85]. Later, this analogy was extended to trajectory-based tasks, like goal-crossing [67] and steering [66], leading to the formulation of Equation 6 in 2D environments. However, 3D environments introduce an additional dimension of trajectory deviation perpendicular to the direction of movement (see Figure 1-d). This motivates us to evaluate the applicability of effective throughput in 3D steering and to compare alternative approaches, toward proposing an empirically validated method that strengthens the foundation for future work.

To calculate the trajectory spread for the effective width, the straightforward approach is to use the univariate standard deviation

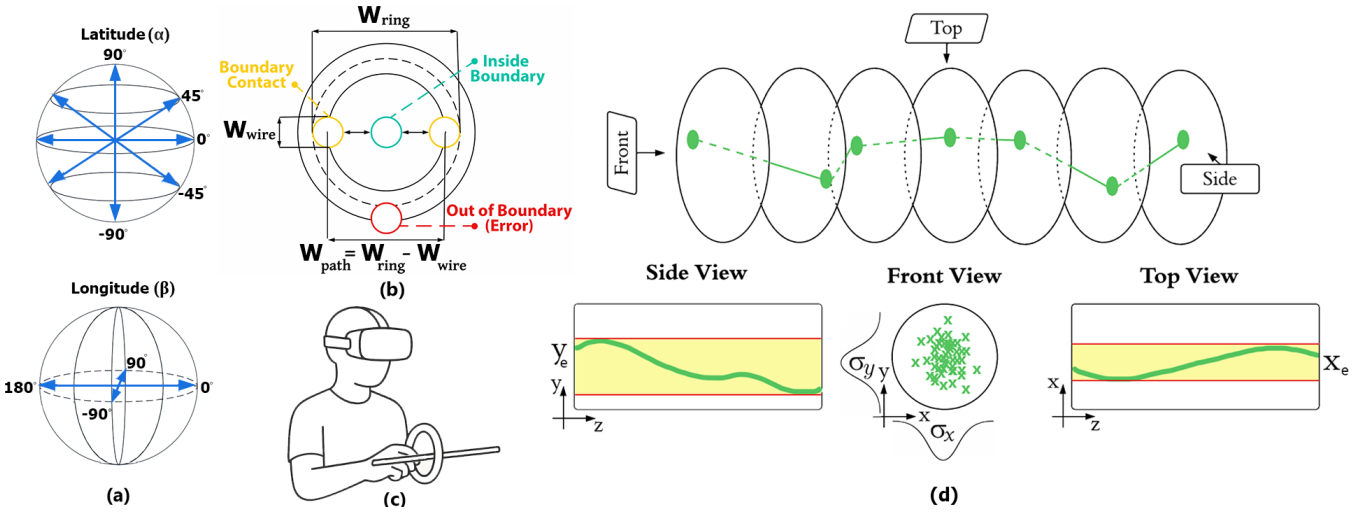

Figure 1: (a) Latitude–longitude mapping of path endpoints used to define 18 unique 3D orientations in the study, including main axial and diagonal orientations that lie on the Cartesian planes. (b) Definition of path width (W_{Path}), derived from the ring and wire geometry (W_{Ring}, W_{Wire}), representing the available movement space orthogonal to the path direction. Also, different ring and wire positional states are indicated: inside-boundary movement (green), boundary contact (yellow), and going out of boundary, i.e., a task error (red). (c) Illustration of the experimental task. (d) Illustration of effective parameters in 3D steering. The task is conceptualized as an infinite series of goal-crossings, with z as the path direction and x–y forming the two orthogonal axes (σ_x and σ_y denote the trajectory spread along these axes, respectively). The green dots show the trajectory points of the ring in an example movement.

of trajectory coordinates on the local plane orthogonal to task axis, i.e., direction of movement, using Equation 7, where $r_i = \sqrt{x_i^2 + y_i^2}$, x and y represent the local axes orthogonal to task axis [66, 67]. However, this method oversimplifies the trajectory spread when variability is not evenly distributed across the two axes orthogonal to the task axis (see Figure 1-d, front view). Therefore, we propose calculating the effective width using the bivariate standard deviation method similar to the calculation suggested by Wobbrock et al. [132] (see Equation 8). Also, as the steered trajectory forms a 3D sample cloud within the path volume, a trivariate standard deviation could be an appropriate candidate for capturing its full volumetric spread: x and y represent orthogonal deviation, z is the progress along the task axis, and compute σ_{xyz} following Equation 9. Including this formulation allowed us to test whether this analogy extends to effective parameters in 3D steering.

$$\sigma_r = \sqrt{\frac{\sum_{i=1}^{n}(r_i - \bar{r})^2}{n-1}} \tag{7}$$

$$\sigma_{xy} = \sqrt{\frac{\sum_{i=1}^{n}\left[(x_i - \bar{x})^2 + (y_i - \bar{y})^2\right]}{n-1}} \tag{8}$$

$$\sigma_{xyz} = \sqrt{\frac{\sum_{i=1}^{n}\left[(x_i - \bar{x})^2 + (y_i - \bar{y})^2 + (z_i - \bar{z})^2\right]}{n-1}} \tag{9}$$

Effective Amplitude (A_e) accounts for the traversed distance along the task axis in pointing studies [18, 67, 85]. Extending this to 2D steering, Kasahara et al. [66] showed that A_e should be calculated as the average steered distance in 2D. As shown in Figure 1-d, in 3D, we propose A_e as the total trajectory amplitude traversed in 3D space. In the trivariate calculation of effective width, the standard deviation of the trajectory is considered across all three dimensions, reflecting the movement variability in 3D. However, for the univariate and bivariate candidates, similar to the previous work [66, 67], we calculated effective ID and throughput both with the nominal A_n (Univariate: $ID_{e,uni\text{-}An}$, $TP_{e,uni\text{-}An}$. Bivariate: $ID_{e,bi\text{-}An}$, $TP_{e,bi\text{-}An}$) and effective A_e (Univariate: $ID_{e,uni}$, $TP_{e,uni}$. Bivariate: $ID_{e,bi}$, $TP_{e,bi}$), to explore a wider range of alternative formulations and study their effects separately. In addition, as Kasahara et al. [66] highlighted, we compute standard deviations within each trial.

4 User Study

4.1 Participants

Using G*Power [34], we conducted an a priori power analysis (α = .05, power = .95, and a large effect size η^2 = .14 based on a pilot study), which indicated that at least 18 participants were required for an RM-ANOVA. We accordingly recruited 18 participants (9 female, 9 male), aged 23–31 years (M = 25.78, SD = 2.58), with varying XR and 3D gaming experience. Participants were volunteers recruited from the university and the general public through online flyers. All but three were right-handed, and all had normal or corrected-to-normal vision. We also ensured that each participant's arm length matched the maximum path length, allowing them to reach all path conditions without adjusting their seated position.

4.2 Apparatus

We used an Intel(R) i7-12700F processor running at 2.1 GHz, 16 GB of RAM, and an NVIDIA GeForce RTX 3060 Ti GPU. The virtual models were created in Blender 4.2, while the VR system was developed in Unity 2022.3.49f1 with the Meta XR All-in-One SDK 68.0.1. For the VR Head-Mounted-Display (HMD), we used a Meta Quest 3.

4.3 Procedure

After signing the consent form and completing a demographic survey, participants were briefed on the study. Participants completed a set of training trials until they became comfortable with the task, which took less than five minutes per participant, as the task is straightforward. At the beginning of the study, participants initiated the task by clicking a start button, which centered the scene in front of the participants. Following Amini et al.'s [9] recommendation, we employed the *"Ring and Wire"* task (see Figure 1-c), isolating translational movement, since it offers a reliable measure of motor control with clear path constraints.

Participants, seated and using their dominant hand [9, 78, 128, 129], first grabbed a ring placed 2.5 cm before the wire's start, which ensured any grasping jitter occurred outside the recorded steering phase [9]. A semi-transparent virtual hand supported spatial awareness during reaching [121, 125], but once the ring entered the wire's start point (marking the beginning of steering), the hand became invisible to avoid distraction and occluding the path's boundaries [9, 46, 121]. Participants then steered the ring along the wire to the endpoint.

Following previous speed-accuracy trade-off studies [18, 66, 67, 138, 142], we introduced three verbal task-execution biases (Fast, Fast & Accurate, and Accurate) and displayed the current bias in the top-left corner of the scene as a reminder. Although some pointing studies [87, 95] used extreme execution biases, e.g., max-speed or max-accuracy, we did not adopt such conditions because they are less informative for evaluating device or user performance in typical interaction settings [66, 67], where participants are generally instructed to perform 'as fast and as accurate as possible' [2, 18, 111].

All conditions were aligned to a common reference point, i.e., 15 cm below and 35 cm in front of the headset, maintaining a consistent visual scale. We adopted this location as it was previously identified as a comfortable position for mid-air steering [9]. Trials were presented one by one, with steering performance recorded from the moment the ring entered the path until it reached the end. The next trial then appeared automatically in front of the participant. Following prior 2D [3, 66, 135, 139] and 3D [9, 78, 128, 129] Steering law studies, we used discrete movements and treated each movement as an independent sample to provide a reliable performance estimate [39, 95].

In our study, the ring and wire were not constrained by collision mechanics, as a pre-study had shown that such constraints allowed sliding along the wire independent of actual hand motion. This mismatch could produce unrealistically short steering times, e.g., < 240 ms, below the human reaction time [81], creating ballistic rather than controlled trajectories [67, 70, 89]. Unlike Liu et al. [78], we did not pause the task when boundary violations occurred. Pausing mid-action is uncommon in modern VR interfaces, and prior work shows that interrupting movements reduces the Steering law's predictive accuracy [78]. Similar to prior work [9, 60, 128], we provided continuous feedback to make participants aware of boundary contacts. When the wire touched the boundary, e.g., Figure 1-b, it turned red, and an error tone signaled each impact. If the ring exceeded the path boundary, i.e., lateral offset greater than the available path width Figure 1-b, the trial automatically restarted. A distinct success tone confirmed the completion of each valid trial.

To reduce fatigue and mitigate the gorilla arm effect [52, 62], participants were given mandatory breaks between changes in task execution bias. In total, each session lasted less than one hour.

4.4 Design

To ensure the paths were comfortably reachable, we referred to anthropometric data [112, 144] and conducted a pilot study to confirm that chosen parameters were practical, comfortable, and offered clear task boundaries for the seated participants. We also selected commonly used path lengths and widths for 3D mid-air steering studies [9, 78, 128, 129]. The independent variables are summarized below:

- Task execution bias: speed (Fast), speed and accuracy (Fast & Accurate), and accuracy (Accurate).
- Path Width (W): 0.02, 0.04, and 0.08 m.
- Path Length (L): 0.25 and 0.40 m.
- 18 3D Path Orientations (R0-R17): 6 principal axes and 12 face diagonals, considering bi-directional movements.

Path Width (W) is aligned with previous work [9, 78, 128], and is calculated as the ring's diameter minus the wire thickness (see Figure 1-b). Ring and wire thicknesses were fixed at 1 cm. Two path Lengths (L) and three path widths (W) resulted in 6 unique *ID* levels (*ID*s = 3.125, 5.0, 6.25, 10.0, 12.50, 20.0). To capture the effects of movement direction in 3D mid-air interactions [78, 129], we included path orientations aligned with the main axes and all 45° diagonals. To control for handedness effects [78], each orientation included both movements (left-to-right and right-to-left), resulting in 18 distinct path orientations. We counterbalanced the conditions across participants by randomizing path 3D orientation sequences for each participant and applying a Latin Square design to the other independent variables. Each participant performed all conditions three times (in sequence), resulting in $3\ W \times 2\ L \times 18\ Orientations \times 3\ ExecutionBiases \times 3\ repetitions = 972\ trials$.

We recorded task execution time (s), candidate throughput calculations (s^{-1}), and average speed (m/s) for each trial. Since we permitted boundary contact, we captured both the number of boundary contacts and contact time (the duration of boundary contact). This distinction enables us to separate total steering time into steering time within and on the boundaries, enabling a more granular analysis of control behavior. Again, if the ring was pushed outside of the boundary, e.g., Figure 1-b, this indicated a large deviation from the path.

For each frame, we recorded the wire's position relative to the ring in local coordinates, yielding track points for trajectory analysis. We also captured the 3D movement offset per frame to compute speed (offset divided by frame time) and total trajectory distance.

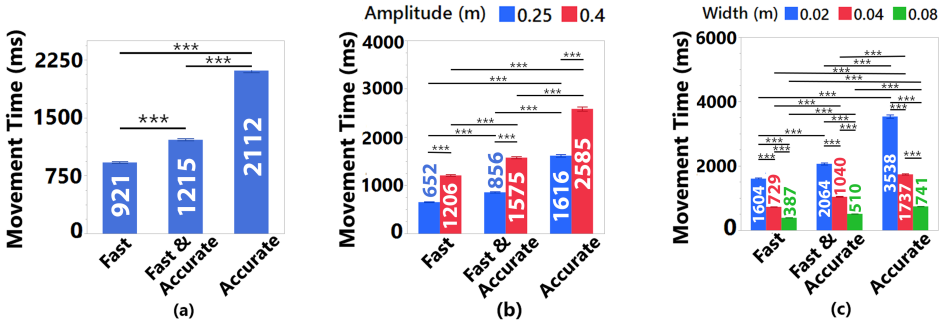

Figure 2: Bar plots of movement time across execution biases (Fast, Fast & Accurate, and Accurate), (a) overall, (b) by path amplitude (0.25 m, 0.40 m), and (c) by path width (0.02 m, 0.04 m, 0.08 m). In this paper, error bars in plots represent Standard Error of the Mean (SEM), and pairwise significant differences are indicated with * (p < .05), ** (p < .01), and * (p < .001).**

5 Results

We used Repeated Measures (RM) ANOVAs ($\alpha = .05$) on all dependent variables to test main effects and interactions using SPSS 31.0. Normality was assumed when Skewness or Kurtosis fell within ±1 [43]; otherwise, we applied log transforms. When sphericity was violated, we used Greenhouse–Geisser corrections. Post-hoc pairwise tests used Bonferroni-adjusted p-values.

5.1 Movement Time (*MT*)

The results showed that *MT* increased with execution bias, reflecting the expected speed-accuracy trade-off, meaning Accurate was slowest ($M = 2112$ *ms*, $SD = 840$), followed by Fast & Accurate ($M = 1215$ *ms*, $SD = 1021$), and Fast ($M = 921$ *ms*, $SD = 1898$) (see Table 1). Interaction results showed that execution bias depended on path width and length (see Figure 2), highlighting that tighter or longer constraints amplify performance costs.

5.2 Error Rate (*ER*)

To assess accuracy, we first analyze *ER* as the proportion of failed trials, i.e., the number of instances where the ring left the path boundary (i.e., exceeded the available path width, as shown in Figure 1-b) relative to the total number of trials. The results showed that *ER* decreased as execution bias shifted toward accuracy, with Fast having the highest *ER* ($M = 25.60$ %, $SD = 43.64$), followed by Fast & Accurate ($M = 17.90$ %, $SD = 38.36$), while Accurate led to the lowest *ER* ($M = 10.10$ %, $SD = 30.16$) (see Table 1). Interaction effects indicated that *ER* was sensitive to path width and length (see Figure 3). Narrower and longer paths amplified the accuracy cost of speed-oriented strategies, consistent with the trade-offs predicted.

5.3 Average Boundary Contacts

To assess how long participants were in contact with the path boundaries, we calculated the ratio of contact time to MT, and overall, only 7.3% of each trajectory was in contact with the boundary. Also, to further investigate contacts, we analyzed average boundary contacts, i.e., the number of times the ring contacted the wire without leaving the available width, e.g., Figure 1-b. Unlike ER, which reflects failed trials, boundary contact captures corrective behavior during successful steering. This distinction is important in 3D steering tasks, where the boundary is a transparent volumetric surface rather than a line, allowing participants to use boundary feedback to adjust their movement without making errors.

As shown in Table 1 and Figure 4, Fast produced the most boundary hits ($M = 0.78$, $SD = 0.98$), followed by Fast & Accurate ($M = 0.71$, $SD = 0.98$), and Accurate ($M = 0.53$, $SD = 0.94$). Longer paths increased contacts across all bias conditions. Narrow paths ($W = 2$ cm) also yielded substantially more hits than medium ($W = 4$ cm) or wide ($W = 8$ cm) paths, where contacts were nearly nonexistent.

5.4 Trajectory Analysis

Assuming a Gaussian distribution [18, 87], effective throughput reflects actual performance by using the observed spread of trajectory points rather than nominal task parameters. To examine this assumption and characterize trajectory variability, we visualized the steering spread along the two axes perpendicular to the task axis as 2D density maps (see Figure 5), where each map shows the trajectory distribution. Except for depth movements (where depth is the task axis, and x and y represent vertical and lateral motion), the horizontal x-axis denotes relative depth deviation (larger values indicate greater distance from the user). Trials were grouped by path orientation to compare trajectory characteristics across conditions.

As shown in Figure 5, trajectory analysis revealed patterns in how task execution bias and path width changed movement variability. Across many conditions, the variability was elliptical (e.g., Figure 5: depth movements, Accurate, and $W = 4$ cm) with the principal axis rotated, often diagonally (e.g., Figure 5: lateral movements, Fast, $W = 4$ cm) rather than circular (e.g., Figure 5: depth movements, Accurate, $W = 8$ cm). Path orientation in 3D space also affected these distributions, i.e., the "Vertical", "Lateral", "Depth", and "Diagonal" subsets showed distinct spread visualizations, movements in depth showed more circular spread, whereas vertical and lateral movements were more asymmetric and angled, respectively.

Trials lying on the image plane, i.e., the plane perpendicular to the viewing angle, resulted in longer spread along the x-axis (depth), which is clearer when we extract the main axial movements. This

Table 1: Repeated-measures ANOVA results for movement time, error rate, and average boundary contacts across Execution bias (E), path Width (W), path Length (L), and their interactions (significant ones highlighted).

	Movement Time			Error Rate			average boundary contacts		
Effect	F	p	η^2	F	p	η^2	F	p	η^2
E	F(1.43,24.40) = 93.890	<.001	0.847	F(2,34) = 62.717	<.001	0.787	F(1.45,24.61) = 42.40	<.001	0.714
W	F(1.57,26.67) = 1264.148	<.001	0.987	F(1.23,20.85) = 170.739	<.001	0.909	F(1.21,20.60) = 1277.235	<.001	0.987
L	F(1,17) = 880.677	<.001	0.981	F(1,17) = 78.190	<.001	0.821	F(1,17) = 786.190	<.001	0.979
ExW	F(4,68) = 3.684	0.009	0.178	F(2.23,37.98) = 15.166	<.001	0.471	F(2.71,46.05) = 14.151	<.001	0.454
ExL	F(2,34) = 3.927	0.029	0.188	F(2,34) = 1.077	0.352	0.06	F(2,34) = 5.191	0.011	0.06
WxL	F(1.39,23.57) = 3.790	0.05	0.035	F(1.29,21.94) = 5.331	0.023	0.239	F(1.10,18.89) = 176.423	<.001	0.912
ExWxL	F(4,68) = 1.671	0.167	0.09	F(4,68) = 0.990	0.419	0.055	F(2.27,38.65) = 3.435	0.037	0.168

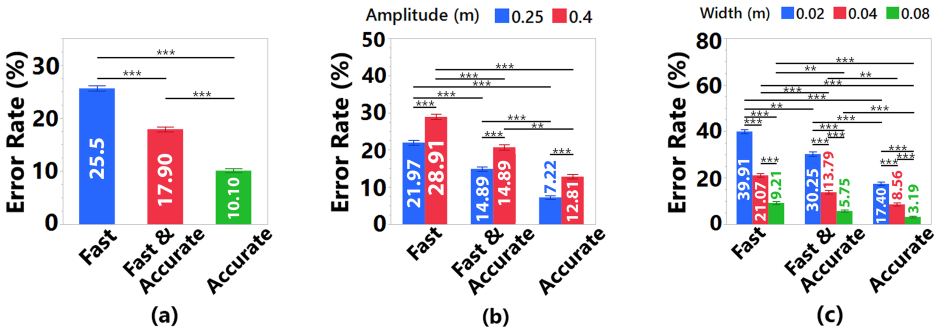

Figure 3: Bar plots of error rate across execution biases (Fast, Fast & Accurate, and Accurate): (a) overall, (b) by path amplitude (0.25 m, 0.40 m), and (c) by path width (0.02 m, 0.04 m, 0.08 m).

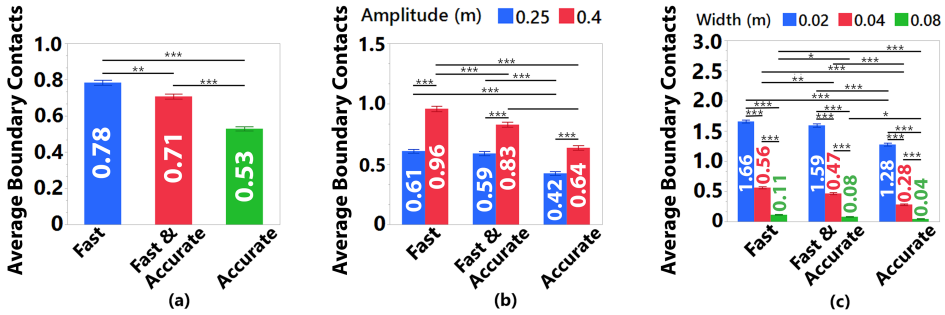

Figure 4: Bar plots of average boundary contacts across execution biases (Fast, Fast & Accurate, and Accurate): (a) overall, (b) by path amplitude (0.25 m, 0.40 m), and (c) by path width (0.02 m, 0.04 m, 0.08 m).

larger deviation along the depth axis can also be seen in vertical and lateral movements.

Overall, at the narrowest width (2 cm), trajectories often traced the path boundary (e.g., Figure 5: all image-plane paths, Fast, $W = 2$ cm). As the width increased, boundary contacts decreased, and wide paths (8 cm) produced compact interior density clouds with minimal contact, especially under accuracy-focused conditions. Particularly, for movement parallel to the image plane (vertical, lateral, diagonal), boundary contacts were concentrated along the depth axis (see Figure 5).

5.5 Throughput (TP)

We analyzed all candidate *TP* calculations using RM-ANOVA (see Table 2) and further examined their stability across task execution biases and task difficulty levels.

5.5.1 Across Speed-Accuracy Biases. To assess throughput stability across speed–accuracy biases, we first followed prior work and tested whether any calculation fully removed speed–accuracy effects using a permutation test [66], where we compared pairs of throughput calculations (e.g., TP_{n} vs. $TP_{\text{e,bi-An}}$) across bias pairs (e.g., Fast vs. Accurate). All comparisons showed significant differences between execution biases (see Figure 6), indicating that

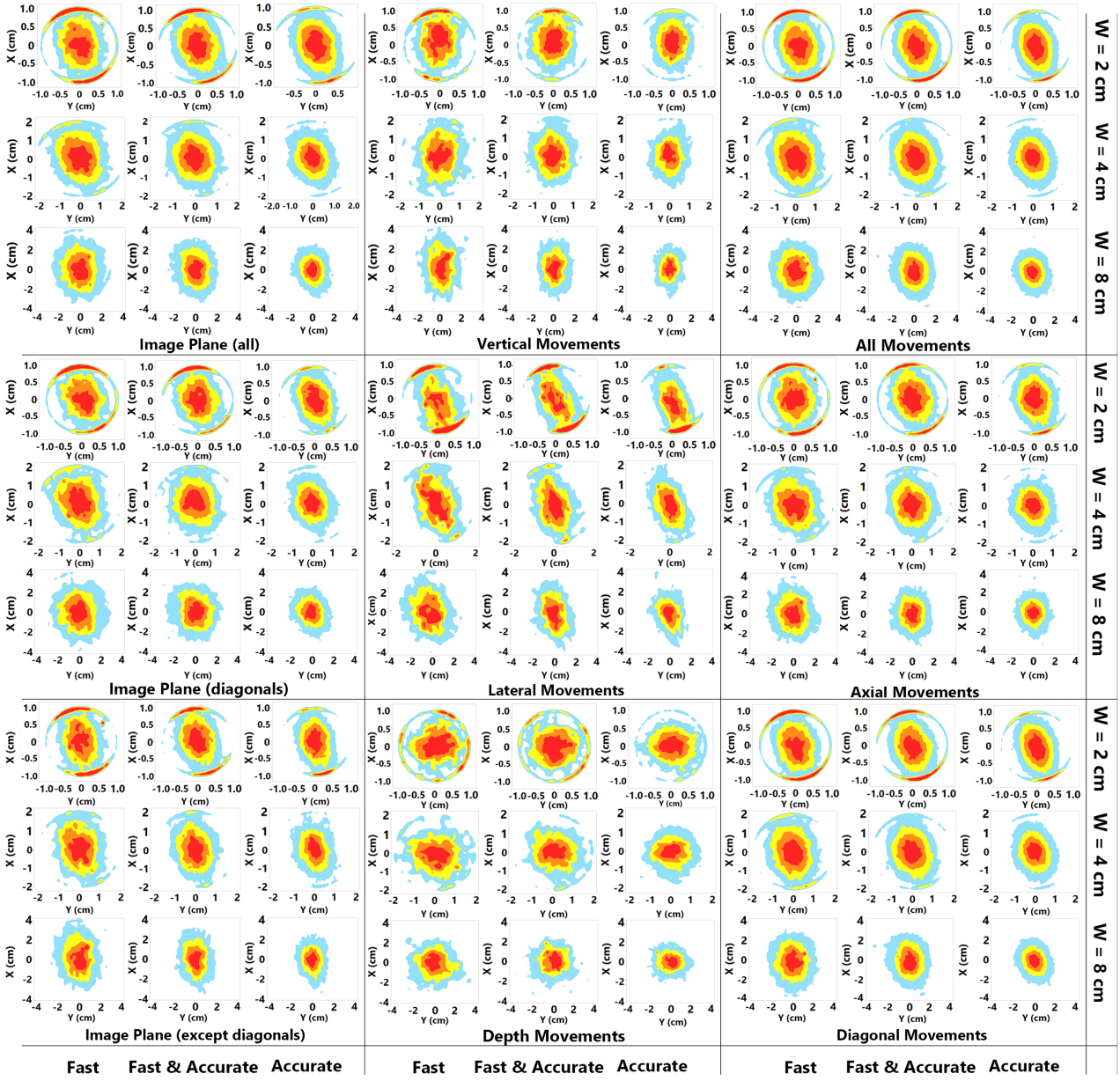

Figure 5: Density heatmaps of trajectories orthogonal to the direction of movement, shown in local coordinates, indicating the actual area used within the nominal path width across execution biases (Fast, Fast & Accurate, Accurate), path widths (2 cm, 4 cm, 8 cm), and movement orientations (image plane, vertical, lateral, depth, axial, and diagonal). The horizontal x-axis denotes depth (larger x values correspond to positions further from the user), unless depth is the primary movement direction.

none of the candidate throughput definitions fully eliminated the speed–accuracy trade-off.

Furthermore, to examine how different effective parameter calculations reduce variability, we followed prior work [66, 67, 95] and computed the TP relative difference ($(TP_{\max} - TP_{\min})/TP_{\max} \times 100\%$). Lower values indicate greater stability. This metric was 44.74% and 20.69% for 2D crossing tasks with directional and amplitude constraints [67], and in 2D linear steering, it decreased from

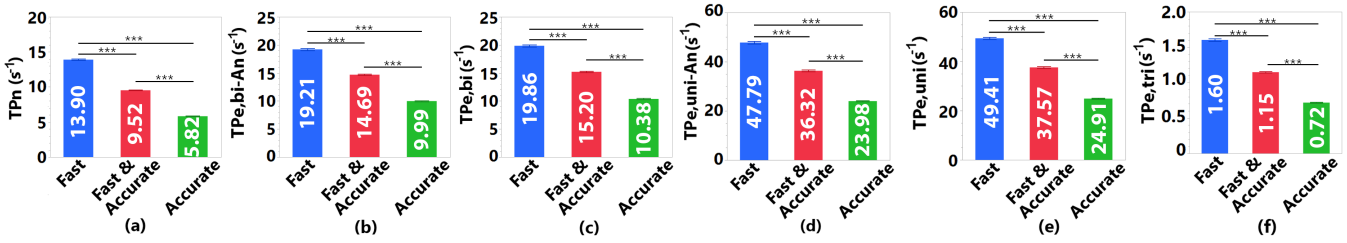

Figure 6: Bar plots of throughput across execution biases (Fast, Fast & Accurate, and Accurate) based on calculation methods (nominal TP_{n} (a), bivariate $TP_{e,bi\text{-}An}$ (b) and $TP_{e,bi}$ (c), univariate $TP_{e,uni\text{-}An}$ (d) and $TP_{e,uni}$ (e), and trivariate $TP_{e,tri}$ (f)).

Table 2: Repeated-measures ANOVA results for throughput (significant ones highlighted) across Execution bias (E), path Width (W), path Length (L), and their interactions, based on different effective parameter formulations (nominal TP_{n}, univariate $TP_{e,uni\text{-}An}$ and $TP_{e,uni}$, bivariate $TP_{e,bi\text{-}An}$ and $TP_{e,bi}$, and trivariate $TP_{e,tri}$).

	TP_{n}			$TP_{e,bi\text{-}An}$			$TP_{e,bi}$		
Effect	F	p	η^2	F	p	η^2	F	p	η^2
E	F(1.41,24.01) = 36.940	<.001	0.831	F(1.48,25.12) = 67.143	<.001	0.798	F(1.46,24.97) = 66.191	<.001	0.796
W	F(1.44,24.50) = 1.137	0.333	0.063	F(1.52,25.86) = 428.256	<.001	0.962	F(1.53,26.05) = 432.667	<.001	0.962
L	F(1,17) = 41.284	<.001	0.708	F(1,17) = 207.168	<.001	0.924	F(1,17) = 218.093	<.001	0.928
ExW	F(4,68) = 0.630	0.643	0.036	F(4,68) = 3.064	0.022	0.26	F(4,68) = 2.795	0.033	0.141
ExL	F(2,34) = 3.386	0.046	0.271	F(2,34) = 4.411	0.02	0.271	F(2,34) = 4.563	0.018	0.212
WxL	F(1.55,26.36) = 0.824	0.447	0.046	F(1.54,26.21) = 3.571	0.039	0.174	F(2,34) = 4.109	0.025	0.195
ExWxL	F(4,68) = 0.690	0.601	0.039	F(4,68) = 1.263	0.293	0.069	F(4,68) = 1.309	0.275	0.072
	$TP_{e,uni\text{-}An}$			$TP_{e,uni}$			$TP_{e,tri}$		
Effect	F	p	η^2	F	p	η^2	F	p	η^2
E	F(1.44,24.60) = 71.019	<.001	0.807	F(1.43,24.46) = 70.142	<.001	0.805	F(1.42,24.17) = 86.88	<.001	0.836
W	F(1.45,24.66) = 400.81	<.001	0.959	F(1.46,24.83) = 406.397	<.001	0.96	F(1.38,23.61) = 936.266	<.001	0.982
L	F(1,17) = 217.587	<.001	0.928	F(1,17) = 228.289	<.001	0.931	F(1,17) = 872.830	<.001	0.981
ExW	F(4,68) = 8.222	<.001	0.326	F(4,68) = 7.957	<.001	0.319	F(4,68) = 0.957	0.437	0.053
ExL	F(2,34) = 3.025	0.062	0.151	F(2,34) = 3.135	0.056	0.156	F(2,34) = 2.429	0.103	0.125
WxL	F(2,34) = 1.170	0.323	0.064	F(2,34) = 1.369	0.268	0.075	F(2,34) = 1.174	0.321	0.065
ExWxL	F(4,68) = 0.602	0.662	0.034	F(4,68) = 0.633	0.641	0.036	F(4,68) = 0.905	0.466	0.051

68.6% for nominal throughput to 53.30% and 53.80% when using effective width alone or combined with effective amplitude [66]. In our study (see Table 3), the relative difference was highest for TP_{n} (58.13%) and lowest for $TP_{e,bi}$ (47.70%), followed closely by $TP_{e,bi\text{-}An}$ (48.02%).

5.5.2 Across Task Difficulties. We assessed throughput stability across task difficulties using the Coefficient of Variation (CV) [66, 85], computed as the ratio of standard deviation to mean for each calculation in each execution condition (lower CV indicates greater stability). As shown in Table 3, nominal throughput (TP_{n}) produced the lowest CVs across all biases, while effective formulations yielded higher CVs. Among them, the bivariate measures ($TP_{e,bi}$ and $TP_{e,bi\text{-}An}$) showed consistently lower variability than the univariate versions ($TP_{e,uni}$, $TP_{e,uni\text{-}An}$) and outperformed the trivariate measure in Fast and Accurate conditions. Between the two bivariate variants, $TP_{e,bi}$ was the most stable across task difficulties.

5.6 Model-Fit

We compared linear fits of the Steering law using different calculations of effective *ID*. As shown in Table 4 and Figure 7, we conducted two analyses, one treating each execution bias separately, i.e., Fast, Fast & Accurate, or Accurate, and one combining all data points across biases (Mixed). We report the non-adjusted R^2 values as all regression models in our analysis include only a single explanatory variable (*ID*) [63, 115]. Overall, the nominal *ID* (ID_{n}) provided a good model-fit in bias-separated conditions (e.g., R^2 = .99 in Fast), but dropped sharply when biases were Mixed (R^2 = .70), confirming sensitivity to subjective speed-accuracy trade-offs.

For effective width formulations, both the bivariate ($ID_{e,bi\text{-}An}$) and univariate ($ID_{e,uni\text{-}An}$) approaches provided similar strong linear fits across execution biases. However, the $ID_{e,bi\text{-}An}$ model provides a stronger model-fit in the Mixed condition, highlighting that the bivariate effective width calculation yields a more accurate fit when varying subjective speed–accuracy strategies are present. In contrast, trivariate formulations ($ID_{e,tri}$) consistently underperformed, with reduced R^2 (.66 – .89) in both bias-separated and

Table 3: Summary of relative difference between minimum and maximum throughput values of throughput calculations to assess stability across speed–accuracy biases. As for the stability across task difficulties, the coefficient of variation (CV) is reported for each throughput formulation (nominal $TP_{\mathbf{n}}$, univariate $TP_{\mathbf{e,uni\text{-}An}}$ and $TP_{\mathbf{e,uni}}$, bivariate $TP_{\mathbf{e,bi\text{-}An}}$ and $TP_{\mathbf{e,bi}}$, and trivariate $TP_{\mathbf{e,tri}}$).

		TP_{n}	$TP_{\mathrm{e,bi\text{-}An}}$	$TP_{\mathrm{e,bi}}$	$TP_{\mathrm{e,uni\text{-}An}}$	$TP_{\mathrm{e,uni}}$	$TP_{\mathrm{e,tri}}$
Relative Variability	Across Biases	58.13 %	48.02 %	47.70 %	49.82 %	49.58 %	55.28 %
Coefficient of Variation	Fast	59.72 %	73.03 %	72.25 %	76.85 %	76.06 %	76.49 %
	Fast & Accurate	44.75 %	77.88 %	76.46 %	80.55 %	79.06 %	73.68 %
	Accurate	43.81 %	73.92 %	72.25 %	79.35 %	77.77 %	77.97 %

Table 4: Steering law model fits across separate execution biases (Fast, Fast & Accurate, and Accurate), as well as in a mixed manner (Mixed), reported for different formulations of the index of difficulty (nominal $ID_{\mathbf{n}}$, univariate $ID_{\mathbf{e,\ uni\text{-}An}}$ and $ID_{\mathbf{e,uni}}$, bivariate $ID_{\mathbf{e,bi\text{-}An}}$ and $ID_{\mathbf{e,bi}}$, and trivariate $ID_{\mathbf{e,tri}}$) with regression equations and R^2 values.

Model	Execution Bias	Equation	R^2	Model	Execution Bias	Equation	R^2
ID_{n}	Fast	$MT = -72 + 105\ ID_{\mathrm{n}}$	0.99	$ID_{\mathrm{e,uni\text{-}An}}$	Fast	$MT = -1101 + 75\ ID_{\mathrm{e,uni\text{-}An}}$	0.98
	Fast & Accurate	$MT = -43 + 133\ ID_{\mathrm{n}}$	0.98		Fast & Accurate	$MT = -1808 + 106\ ID_{\mathrm{e,uni\text{-}An}}$	0.98
	Accurate	$MT = -87 + 227\ ID_{\mathrm{n}}$	0.99		Accurate	$MT = -3377 + 178\ ID_{\mathrm{e,uni\text{-}An}}$	0.93
	Mixed	$MT = -67 + 155\ ID_{\mathrm{n}}$	0.7		Mixed	$MT = -2083 + 116\ ID_{\mathrm{e,uni\text{-}An}}$	0.79
$ID_{\mathrm{e,bi\text{-}An}}$	Fast	$MT = -1156 + 191\ ID_{\mathrm{We}}$	0.98	$ID_{\mathrm{e,uni}}$	Fast	$MT = -1068 + 70\ ID_{\mathrm{e,uni}}$	0.98
	Fast & Accurate	$MT = -1719 + 253\ ID_{\mathrm{We}}$	0.97		Fast & Accurate	$MT = -1726 + 99\ ID_{\mathrm{e,uni}}$	0.98
	Accurate	$MT = -2815 + 374\ ID_{\mathrm{We}}$	0.93		Accurate	$MT = -3226 + 165\ ID_{\mathrm{e,uni}}$	0.94
	Mixed	$MT = -2123 + 298\ ID_{\mathrm{We}}$	0.86		Mixed	$MT = -2145 + 123\ ID_{\mathrm{e,uni}}$	0.78
$ID_{\mathrm{e,bi}}$	Fast	$MT = -1121 + 181\ ID_{\mathrm{e,bi}}$	0.98	$ID_{\mathrm{e,tri}}$	Fast	$MT = -15305 + 20134\ ID_{\mathrm{e,tri}}$	0.89
	Fast & Accurate	$MT = -1645 + 236\ ID_{\mathrm{e,bi}}$	0.97		Fast & Accurate	$MT = -24194 + 31149\ ID_{\mathrm{e,tri}}$	0.88
	Accurate	$MT = -2693 + 348\ ID_{\mathrm{e,bi}}$	0.95		Accurate	$MT = -50849 + 64368\ ID_{\mathrm{e,tri}}$	0.84
	Mixed	$MT = -2051 + 279\ ID_{\mathrm{e,bi}}$	0.89		Mixed	$MT = -27219 + 35132\ ID_{\mathrm{e,tri}}$	0.66

Mixed conditions. These results suggest that while trivariate approaches may attempt to capture 3D variability, they decrease the predictive power of the Steering law, making them less suitable for modeling 3D motor performance using the Steering law.

When effective amplitude (A_{e}) was incorporated, both the univariate ($ID_{\mathrm{e,uni}}$) and bivariate ($ID_{\mathrm{e,bi}}$) formulations provided strong model fits, but were comparable with $ID_{\mathrm{e,bi\text{-}An}}$ and $ID_{\mathrm{e,uni\text{-}An}}$ (which use nominal values of amplitude) in the separated-bias comparison. Yet, the Mixed condition, replacing nominal values with A_{e} in the $ID_{\mathrm{e,bi\text{-}An}}$ calculation, increased R^2 values. Also, calculating $ID_{\mathrm{e,bi}}$ using the bivariate standard deviation and A_{e}, outperformed its univariate counterpart ($ID_{\mathrm{e,uni}}$) when execution biases were combined.

5.7 Effective Width of Traversed Trajectory

RM-ANOVA (see Table 5) showed significant main effects of execution bias, path width, and path length on effective width ($W_{\mathrm{e,bi}}$). $W_{\mathrm{e,bi}}$ decreased with higher accuracy demands, narrower widths, and longer paths, indicating tighter control under more difficult conditions. Significant interactions emerged between execution bias and length, and between width and length. No interaction between execution bias and width was found.

We analyzed Zhai et al.'s index of utilization ($I_{\mathrm{u}} = \log_2(W_{\mathrm{e,bi}}/W)$), indicating how much of the path width participants used [148]. Values near zero indicate full use of the nominal width, whereas negative values reflect narrower effective use. The RM-ANOVA (see Table 5) showed significant main effects of execution bias, width, and length, along with two-way interactions. As shown in Figure 8, I_{u} was consistently below zero across biases, indicating that participants generally steered within a narrower region than the available width. Execution bias had a strong effect: Fast yielded the largest (least negative) I_{u}, whereas Accurate produced the smallest values, reflecting tighter control (see Figure 8-a). Length also affected utilization, shorter paths produced smaller I_{u}, indicating greater utilization in longer paths (see Figure 8-b).

Similarly, width affected I_{u}. Participants used nearly the full width for 2 cm paths, while utilization decreased in wider paths, especially under accuracy-focused conditions (see Figure 8-c). We also observed that I_{u} increased with task difficulty across execution biases (see Figure 8-d), and the differences between Fast, Fast & Accurate, and Accurate widened as difficulty increased, indicating higher utilization in harder tasks.

5.8 Effective Amplitude of Traversed Trajectory

RM-ANOVA results for A_{e} and $I_{\mathrm{u}}(A_{\mathrm{e}})$ showed significant main effects of execution bias, width, and length on both (see Table 6). $I_{\mathrm{u}}(A_{\mathrm{e}})$ increased with accuracy demands (see Figure 9-a). Accurate yielded the highest utilization ($M = 0.049$), followed by Fast & Accurate ($M = 0.0436$) and Fast ($M = 0.0402$). Path length and width also affected utilization, where narrow and shorter paths yielded higher $I_{\mathrm{u}}(A_{\mathrm{e}})$, indicating higher proportional utilization of the available amplitude. Plotting $I_{\mathrm{u}}(A_{\mathrm{e}})$ against the nominal ID

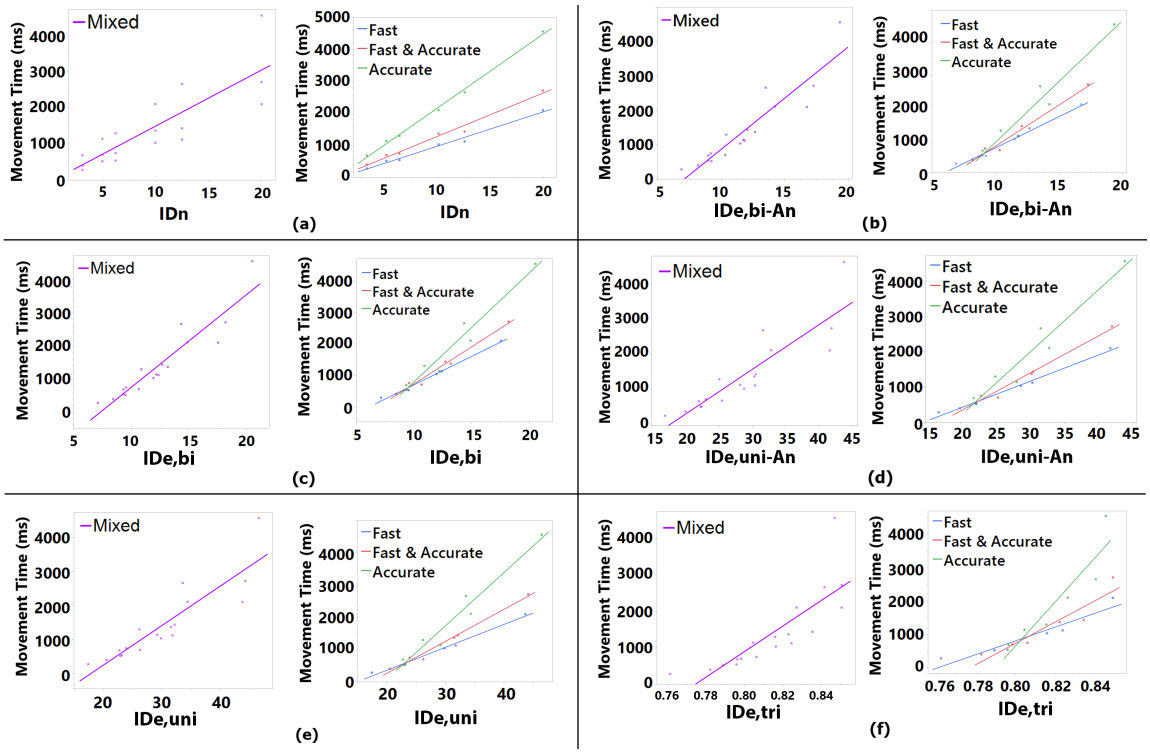

Figure 7: Linear regression plots of movement time against different index of difficulty across execution biases separately (Fast, Fast & Accurate, and Accurate), as well as in a mixed manner (Mixed), reported for different formulations of the index of difficulty (a: nominal ID_n, b: bivariate $ID_{e,bi\text{-}An}$, c: bivariate $ID_{e,bi}$, d: univariate $ID_{e,uni\text{-}An}$, e: univariate $ID_{e,uni}$, f: trivariate $ID_{e,tri}$).

Table 5: Repeated-measures ANOVA results for effective width ($W_{e,bi}$) and index of utilization of effective width ($I_u(W_{e,bi})$) across Execution bias (E), path width (W), path Length (L), and their interactions (significant ones are highlighted).

	$W_{e,bi}$			$I_u(W_{e,bi})$		
Effect	F	p	eta	F	p	eta
E	F(2,34) =57.054	<.001	0.771	F(2,34) = 64.539	<.001	0.792
W	F(1.33,22.60) = 930.314	<.001	0.982	F(2,34) = 3334.534	<.001	0.995
L	F(1,17) = 481.606	<.001	0.966	F(1,17) = 486.197	<.001	0.966
ExW	F(2.62,44.67) = 1.526	0.204	0.082	F(2.30,39.04) = 8.723	<.001	0.339
ExL	F(2,34) = 11.987	<.001	0.414	F(1.50,25.48) = 11.704	<.001	0.408
WxL	F(2,34) = 122.079	<.001	0.878	F(2,34) = 68.519	<.001	0.801
ExWxL	F(4,68) = 2.297	0.068	0.119	F(4,68) = 1.664	0.169	0.089

(see Figure 9-d) showed that utilization increased with task difficulty, with differences between execution biases becoming more pronounced at higher *ID*s. This pattern suggests that participants moved more in difficult tasks and as accuracy was prioritized, increasing A_e, and thus I_u.

5.9 Movement Speed

RM-ANOVAs identified significant main effects of execution bias, path length, and width on average movement speed (see Table 7), along with significant two-way interactions, indicating that strategy effects on speed depended on path geometry. Participants moved fastest in the Fast (M = 0.62 m/s, SD = 0.44), slower in Fast & Accurate (M = 0.44 m/s, SD = 0.29), and slowest in Accurate (M = 0.28 m/s, SD = 0.19). Shorter paths produced faster movements than longer ones, and wider paths enabled higher speeds than narrower widths.

To examine speed variability during steering, we plotted ring speed based on relative path position (see Figure 10). Comparing low and high task difficulties across execution biases revealed that for a given ID_n, speed variability decreased as accuracy demands increased, and across *ID*s, both mean speed and variability increased as ID_n decreased.

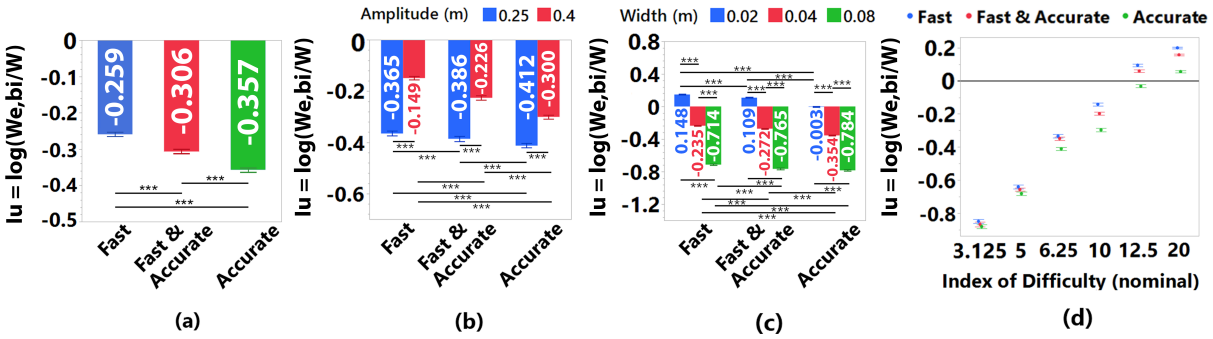

Figure 8: Bar plots of index of utilization of effective width ($I_u(W_{e,bi})$) across execution biases (Fast, Fast & Accurate, and Accurate), (a) overall, (b) by path amplitude (0.25 m, 0.40 m), (c) by path width (0.02 m, 0.04 m, 0.08 m), and (d) across nominal index of difficulty (ID_n).

Table 6: Repeated-measures ANOVA results for effective amplitude (A_e) and index of utilization of effective amplitude ($I_u(A_e)$) across Execution bias (E), path width (W), path length (L), and their interactions (significant ones are highlighted).

	A_e			$I_u(A_e)$		
Effect	F	p	η^2	F	p	η^2
E	F(2,34) = 36.940	<.001	0.685	F(2,34) =55.994	<.001	0.767
W	F(1.26,21.43) = 85.346	<.001	0.834	F(2,34) = 221.182	<.001	0.929
L	F(1,17) = 187189.356	<.001	1.000	F(1,17) = 22.010	<.001	0.564
ExW	F(4,68) = 5.969	<.001	0.260	F(2.35,39.99) = 1.533	0.226	0.083
ExL	F(1.44,24.45) = 6.304	0.005	0.271	F(2,34) = 0.648	0.530	0.037
WxL	F(2,34) = 22.866	<.001	0.574	F(2,34) = 5.253	0.01	0.236
ExWxL	F(4,68) = 0.601	0.663	0.034	F(2.39,40.64) = 0.518	0.632	0.03

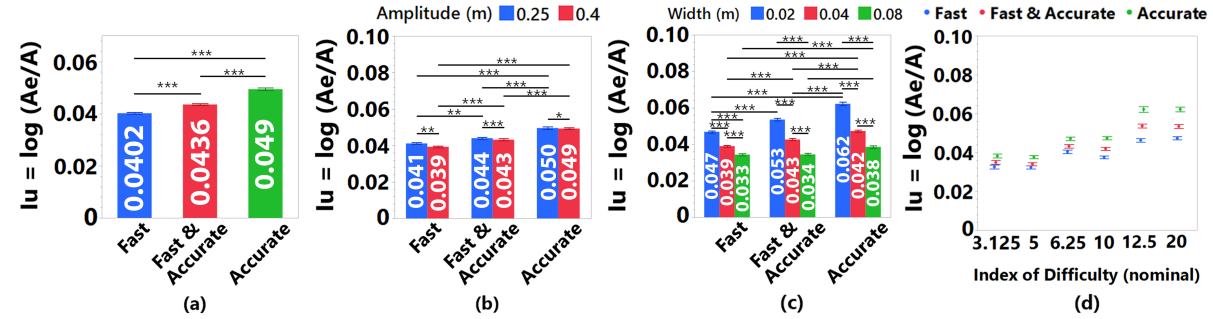

Figure 9: Bar plots of index of utilization of effective amplitude ($I_u(A_e)$) across execution biases (Fast, Fast & Accurate, and Accurate), (a) overall, (b) by path amplitude (0.25 m, 0.40 m), (c) by path width (0.02 m, 0.04 m, 0.08 m), and (d) across nominal index of difficulty (ID_n).

6 Discussion

In this paper, we examined the effective throughput in 3D steering tasks. Our results confirmed that participants consistently followed the intended speed–accuracy biases. Fast produced lower MT, higher speed, more boundary contacts, and higher ER, while Accurate showed the opposite pattern, and Fast & Accurate fell in between. This pattern aligns with established speed–accuracy trade-offs in HCI motor performance research [66, 87, 134] and confirms that our verbal instructions successfully induced distinct execution strategies.

6.1 Effective Parameters Across Speed-Accuracy Biases

Our analysis showed that no formulation fully eliminated the influence of execution strategy, *even after effective adjustments*, though the degree of smoothing differed across formulations. Prior work

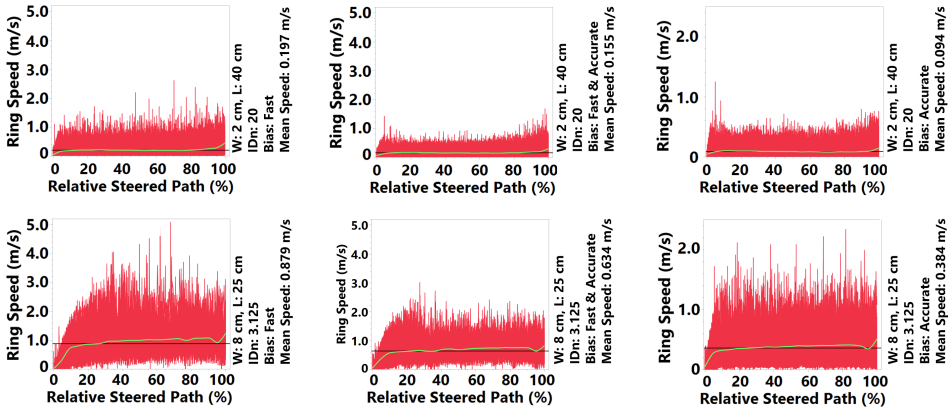

Figure 10: Speed profiles across execution biases (Fast, Fast & Accurate, and Accurate) for highest task difficulty (ID_n = 20, top row) and lowest task difficulty (ID_n = 3.125, bottom row). Red traces show individual trial speeds across participants, and the green line indicates the mean.

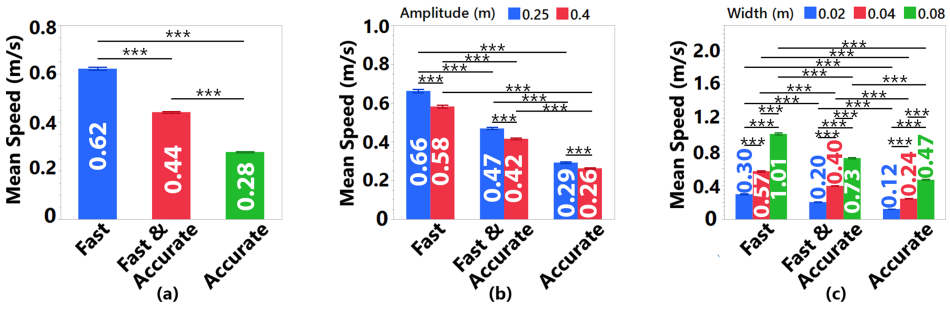

Figure 11: Bar plots of mean speed across execution biases (Fast, Fast & Accurate, and Accurate), (a) overall, (b) by path amplitude (0.25 m, 0.40 m), and (c) by path width (0.02 m, 0.04 m, 0.08 m).

highlighted that perfect invariance to subjective speed–accuracy biases is likely unattainable in 2D [66, 67, 95], which becomes even more pronounced in 3D due to added perceptual and motor demands [15, 18, 19]. Kasahara et al. [66] found that effective parameters do not fully stabilize throughput in 2D steering, but provide fairer comparisons by reducing relative variability across biases.

Table 7: Repeated-measures ANOVA results for average speed across execution bias (E), path width (W), path length (L), and their interactions (significant ones are highlighted).

Effect	F	p	η^2
E	F(1.20,20.40) = 42.17	<.001	0.713
W	F(1.17,19.87) = 268.074	<.001	0.94
L	F(1,17) = 58.067	<.001	0.774
ExW	F(1.96,33.451) = 37.181	<.001	0.686
ExL	F(2,34) = 8.051	<.001	0.321
WxL	F(1.29,22.03) = 4.44	0.019	0.207
ExWxL	F(4,68) = 0.279	0.89	0.016

Overall, TP_n showed the greatest relative variability, while $TP_{e,bi}$ reduced variability across execution biases more than the other calculations. Although TP_n was less variant across task difficulties, consistent with 2D steering [66], it remained highly sensitive to mixed execution biases, limiting its generalizability in HCI user studies, where the speed–accuracy trade-off is an unavoidable factor [18, 27, 67, 87].

The small range of $ID_{e,tri}$ arises from how effective measures are defined. Equation 9 incorporates variability both along and orthogonal to the task axis, yielding larger spread values than other methods (see supplemental material) and compressing $ID_{e,tri}$ into a narrow range. This results in substantially large negative intercepts and small $ID_{e,tri}$, which are not typical in Steering law studies [3, 66, 67, 130], making the trivariate method less discriminative and less suitable for 3D steering.

6.2 Steering Law Model-Fit

Model-fit analysis further supported using $ID_{e,bi}$. When fitting the Steering law under Mixed conditions, ID_n yielded weaker fits, with lower R^2, while $ID_{e,bi}$ improved fit quality compared to other methods, demonstrating its superiority in representing task difficulty under mixed execution strategies.

The observed negative intercepts (a in Equation 2) are common in 2D [2–4, 25, 66, 138] and 3D Steering law studies [78, 120, 129]. Similar to our case, Hoffmann [59] notes negative intercepts are common when modeling steering and often arise from the dataset and *ID* range rather than meaningful motor behavior [111, 137, 146]. Besides, Guiard and Olafsdottir [47, 48] argue that because *MT* cannot be negative and *ID* lacks a true physical zero, intercept values are uninterpretable.

We used six *ID* data points ($2A \times 3W$) for bias-separated linear regressions, which is common in Steering law studies evaluating performance [3] or examining additional task factors [4, 9, 97, 128, 136, 138] beyond path A and W [2, 5]. Although adding more *ID* points, particularly lower than the range in our study, could reduce the likelihood of negative intercepts [137], we selected a range following prior 3D studies [9, 78, 128, 129] to ensure comparability and reflect commonly used spatial constraints.

Still, predictions outside the empirically tested *ID* range should be approached cautiously. At very low or high *ID*s, e.g., extremely wide or narrow paths, the actual *MT* may deviate from the linear model [84, 137, 146], due to participants paying less attention to boundaries in very wide paths or facing extreme precision demands in very narrow ones, altering their movement behavior. In 3D environments, these extremes are further constrained, e.g., very narrow paths may be impractical due to limited boundary perception, while extremely wide paths may reduce engagement with controlled steering.

6.3 Trajectory Variability and Execution Strategies

We further examined factors contributing to the instability of effective throughput to better inform future work. Prior work shows that fast movements (short *MT*) combined with small trajectory variability can greatly increase effective throughput in trajectory-based tasks [66]. Similarly, we observed increased speed and decreased trajectory spreads for lower task difficulties. Higher speed variability across participants is also a source of throughput instability, similar to earlier work [67]. Additionally, unlike 2D steering, where trajectories typically stay well within boundaries even at higher difficulties [66], our results showed clusters of trajectories on boundaries at higher *ID*s, especially under speed-focused conditions. These deviations led to spreads that were neither centered nor normally distributed, even when projected onto a single axis. This underscores how the complexity of 3D mid-air steering can distort distributions to conform (somewhat) less to the normality assumption behind effective parameter calculations.

Our trajectory analysis showed that variability in 3D mid-air steering is anisotropic. Instead of the circular distributions often assumed in pointing [18, 85] and trajectory tasks [66, 67], trajectories were elliptical and angled, particularly on the image plane. This challenges the assumption in many 2D effective throughput studies [66, 67, 84], which model endpoint/trajectory distributions as circular and derive effective width from a univariate spread. While such simplifications are reasonable in 2D, where there is only one axis orthogonal to the movement direction, our results show they do not hold in 3D, where additional perceptual factors and motor constraints change trajectory distributions. One could argue that if variability is dominated by a single axis, dimensionality may be reduced, as in 2D pointing [45, 85]. However, even in 2D, collapsing the data to one dimension can still obscure important aspects of user behavior [132].

Also, the shift of the density centroid away from the geometric path center, typically away from the user, suggests persistent perceptual or postural challenges in mid-air steering [9, 15, 117, 129]. Such offsets underscore the need to compute effective parameters from the actual center of the traversed trajectory rather than the path's center. In our study, elliptical trajectories were not consistently aligned with a single axis across orientations, showing that deviations occurred simultaneously along both orthogonal axes in 3D mid-air steering.

Execution bias significantly affected $I_u(W_{e,bi})$ and average boundary contacts, suggesting that participants adjusted their control strategies, e.g., focusing more on boundary contact cues in harder tasks, especially under Fast, which may contribute to throughput instability. However, we suspect it is not the primary factor. Despite auditory and visual feedback on contact, only 7.3% of *MT* was *on* the boundary, showing that participants did not predominantly rely on boundary sliding.

In a follow-up study (see supplemental material), we compared visual-only (V) feedback with combined visual and auditory feedback (VA) and found no significant differences in performance or trajectory spread, suggesting that steering performance was mainly guided by visual cues, consistent with prior 2D findings [114]. Yet, we only compared V and VA, and alternative mechanisms, e.g., haptic feedback [116, 150] or color mappings [42, 77], may alter the trajectory, but these options are out of scope of this paper. Further, Steering law studies [3, 66, 78, 128] do not require users to stay centered in the path, e.g., in curved paths [66], users may move off-center to shorten the effective path. And, Amini et al. [9] noted that trajectory asymmetries stem from depth overshoot in mid-air steering, further supporting the importance of accounting for the actual trajectory spread, which the bivariate method captures more accurately.

6.4 Spatial Path Constraints

Our findings show that W and L, which define ID_n, significantly affected the effects of execution strategy. Narrower and longer paths increased *MT*, *ER*, and boundary contacts, and these effects interacted with execution bias, indicating that ID_n is not merely additive but shaped by how users choose to steer. In practice, geometric constraints affect speed-accuracy trade-offs; attempting faster movements disproportionately raises errors and boundary hits in narrow or long paths, while emphasizing accuracy yields larger time costs under the same conditions. This also appeared in the trajectory analysis, where we observed orientation-dependent spreads, execution bias interaction with $W_{e,bi}$ and A_e, as well as degraded model-fit under Mixed condition compared to other calculations. Thus, ID_n alone cannot capture such variability, highlighting the essential value of using effective parameters for 3D mid-air steering.

Notably, across most conditions, the mean index of utilization of path width, i.e., $I_u(W_{e,bi})$, remained negative, indicating that participants steered within an area narrower than 96% of nominal

path width. This aligns with an assumption underlying the formulation of effective parameters in previous studies [66, 85], namely that effective width is defined as the spread that encompasses the trajectory with 4% error, further justifying the use of the proposed effective parameters.

Interestingly, $I_u(A_e)$ was higher in ACCURATE, yielding longer effective amplitudes. This contrasts with 2D steering findings, where shorter traversed path and lower $I_u(A_e)$ were reported [66, 67]. Thereby, Kasahara et al. [66] recommended using A_n for linear paths and A_e for more complex shapes in 2D. We believe that this contrast arises because controlled 3D mid-air movements increase interaction control demands due to the lack of physical support [117], increased jitter [19], ambiguous depth cues [15, 21, 58], and/or additional degrees of freedom that amplify unintended deviations, especially in depth [22, 75, 116]. Besides, longer *MT*s can accumulate tremor and movement instability [116], particularly under accuracy-focused strategies that rely on cautious, incremental corrections [18, 84, 85].

Moreover, comparing *ER* and average boundary contacts shows that in FAST, participants produced more failures and more contacts, while emphasizing accuracy reduced both measures, by slowing movements. This is also evident as clusters near boundaries under FAST (see Figure 5), accompanied by higher $I_u(W_{e,bi})$ values, indicate greater utilization of the available width. Taken together, this explains why our A_e results differ from prior 2D linear steering, where A_e and A_n were typically comparable [66, 67]. In FAST, participants produced longer segments with large corrections, and in the ACCURATE condition, they made many fine-grained adjustments along both orthogonal axes. Both behaviors lengthened A_e and increased $I_u(A_e)$, indicating that even linear steering is more complex in 3D, making A_e a more accurate representation of actual movement than A_n. Besides, shorter paths reduced task difficulty, errors, and boundary contacts, and offered less opportunity to deviate from the path, while longer paths increased MT, which may induce greater fatigue [124]. These factors likely enabled participants to complete shorter-path trials faster than longer ones.

6.5 Implications

An important contribution of this work is that it strengthens the methodological foundations of the 3D Steering law. Throughput is a widely used performance metric in HCI [8, 66, 67], yet its use in 3D steering contexts has lacked a justified and empirically evaluated formulation. Our proposed effective throughput measure aims to fill this gap by capturing the trajectory variability more accurately. Based on our findings, we propose the following practical implications:

- We recommend using the nominal ID_n where the distribution of trajectories is unknown, particularly when steering paths are untested or task instructions enforce a specific speed–accuracy trade-off, e.g., "as accurate as possible" in accuracy-critical applications like surgical planning and catheter placement [10, 119], as our results show that ID_n still provides a comparable model-fit when speed–accuracy biases are not mixed in the fitting of *MT* and *ID*.
- In cases where subjective speed–accuracy biases are present and data fitting is performed over mixed conditions, we recommend using the effective $ID_{e,bi}$ calculated with both bivariate effective width ($W_{e,bi}$) and effective amplitude (A_e) for fitting *MT* over *ID* and calculating the effective throughput ($TP_{e,bi}$). This formulation better captures performance differences across mixed task execution strategies, provides a better model-fit, and a smoother throughput across speed-accuracy biases compared to other methods.
- We recommend incorporating varying path orientations in 3D space when evaluating steering tasks. Different orientations lead to distinct trajectory distributions, and combining them ensures a more representative assessment of user performance.

We conducted a follow-up study to assess the practical importance of using effective measures to calculate throughput by comparing two common VR interaction techniques, namely bare hand and controller, both used as a virtual "hand". As shown in the supplemental material, TP_n did not differ significantly, while $TP_{e,bi}$ revealed a significant difference between techniques. TP_n depends only on *MT* and predefined *ID*s, and as *MT* was comparable, TP_n yielded similar results. In contrast, ($TP_{e,bi}$) is calculated from the actual trajectory, where σ_{xy} was significantly different between the two techniques. This is a clear example where $TP_{e,bi}$ reveals underlying performance differences in mid-air steering, which TP_n fails to capture. The most likely cause of the difference is the difference in the tracking methods [41, 82], but this needs to be validated in future work.

The ring-and-wire task has been adopted in 3D interaction studies to evaluate performance, where *MT* and error-related metrics (e.g., path deviation [26] or boundary contacts [26, 42, 53]) were used separately, making it difficult to interpret the outcome, particularly when these metrics change in different directions. For example, Hartbrich et al. [53] found no significant difference in *MT* between hand visualizations in AR, but significantly higher boundary contacts using opaque hands. Also, Christou et al. [26] investigated stroke rehabilitation in VR and reported different changes in *MT* and collisions,e.g., lower *MT* but more collisions. Further, Gemici et al. [42] used a ring-and-wire task in VR to investigate the effect of a Signed Distance Field (SDF) method to support distant object manipulation. They report significant improvements using the SDF in terms of the number of boundary contacts, with no significant improvement in MT, which may obscure whether the SDF is actually improving the performance or not. In such cases, $TP_{e,bi}$ offers a unified indicator of performance, which enables clearer comparisons by combining time and errors into one metric.

Our formulation ($TP_{e,bi}$) attempts to capture the actual trajectory rather than relying on predefined *ID*s. Therefore, we expect it might generalize to a larger variety of steering tasks that share a similar structure, i.e., they have a task axis (the primary direction of movement) and impose constraints along the two orthogonal axes to the task axis, particularly with constant widths, as common in Steering law studies [9, 60, 128]. Such conditions are also common in 3D steering applications, including 3D menus [29–31], cable routing [105, 122], piloting [60], steering through 3D tunnels [9, 68, 71, 78, 128], and medical applications where users navigate an instrument through a constrained path [12, 37, 152]. Amini et al. [9] showed that the ball-and-tunnel tasks used in 3D Steering

law studies [78, 128, 129] result in elliptical trajectory distributions, making our proposed calculation most relevant. In another example, Arikatla et al. [12] assessed laparoscopic surgical training and highlighted that performance depends on balancing path deviation and speed. There, $TP_{e,bi}$ can offer a practical alternative to the separate metrics in their study, i.e., MT and path deviation [12]. Thus, we hope that the new throughput measure will encourage further research toward well-justified and more accurate performance modeling and evaluation of 3D steering.

6.6 Limitations and Future Work

We used a linear ring-and-wire task with varying 3D orientations to isolate the effect of added dimensions of trajectory variability. Introducing more complex shapes, e.g., curved paths or tunnels with varying width, would likely introduce compounding effects and obscure the underlying mechanisms we aimed to study [78]. This control is especially important given the unique perceptual and motor constraints of 3D mid-air interaction [15, 19, 117], which make motor behavior more complex than in 2D.

Also, our study employed discrete bi-directional movements, common in Steering law studies [3, 9, 66, 128]. Yet, the results may not be perfectly identical to a reciprocal task. Participants start and end at different endpoints in the current task, which may have contributed to the asymmetry of trajectories. However, in a reciprocal task, users start and end at the same endpoint. Reciprocal tasks align more closely with Fitts' law studies [8, 85] and would enable a more direct assessment of potential directional effects. This warrants explicit investigations in future work to reveal potential impacts on the outcome.

Aligned with previous work [9, 121], the hand was turned invisible during steering, i.e., after grabbing the ring and entering the path, to reduce visual clutter in our user study. Recent works comparing common virtual hand representations, i.e., invisible, semi-transparent, and opaque, in VR [54, 121, 125] advocated using semi-transparent and invisible hand representations, showing that opaque hands consistently degrade performance and usability due to visual occlusion. Across these studies [54, 121, 125], semi-transparent and invisible hands did not differ significantly in performance. Hatira et al. [54] further confirmed that semi-transparent and invisible hands yielded similar trajectories, movement times, and boundary contacts in a 3D steering task, while opaque rendering led to higher boundary contacts.

In addition, we acknowledge that our VR setup does not faithfully replicate Augmented Reality (AR) scenarios where real-world objects and physical hands are visible. AR introduces additional real-world depth cues, backgrounds, and visual clutter [16, 64]. Batmaz et al. [16] show that although AR users move slightly faster and with fewer corrective movements, these differences do not significantly change movement time, error rate, or Fitts' law effective throughput in 3D space. Recently, using a ring and wire task, Hartbrich et al. [53] showed that different hand visibilities do not yield significant performance differences in AR when interacting with virtual objects, whereas invisible hands lead to fewer boundary contacts and greater ease of interaction when users interact with real objects.

Thus, we speculate that making the hand invisible during steering removes extra visual occlusion cues (and thus potential confounds) without significantly altering the underlying steering behavior, and our findings would likely remain consistent, particularly when hands are semi-transparent in VR. Yet, we did not directly compare different hand visualizations or different environments, and future studies should explicitly investigate such effects to strengthen the external validity of our findings.

Moreover, steering paths may not have constant widths, which limits the applicability of our findings that rely on the uniform-width assumption in current 3D Steering law studies, e.g., [78, 128, 129]. For example, in real-world steering applications, obstacles can be present, and path width can be reduced for short durations [36, 126] or be defined as the negative space between objects [33, 100]. Although using a fixed width aligns with current 3D Steering law studies [78, 128, 129] and provides a clear foundation for our study, it may limit the external validity of our findings. Yamanaka and Miyashita [135] showed that steering through a narrowing tunnel is psychomotorically distinct from steering through a widening one, even when their mean widths are equal. Using the standard deviation of the trajectory aggregates the entire path and may fail to accurately capture movement variability or how users adapt to changing path widths. Future work should therefore investigate 3D steering tasks with varying widths.

Besides, real-world applications in visually cluttered environments can increase the MT by adding visual search time to perceive path boundaries [32, 35, 101]. However, this perceptual bottleneck may not affect trajectory spread, yet it can still reduce $TP_{e,bi}$ by penalizing perceptual load rather than motor steering performance, leading to misleading comparisons between conditions. This still needs to be investigated in future work.

Another application of the Steering law is evaluating tracing task performance [106]. However, target velocity can affect the steering performance while tracing a target in 3D space, making the Steering law insufficient [79, 80]. Thus, solely relying on spatial constraints may not be enough for calculating effective throughput in such applications.

As throughput is widely used to evaluate performance in HCI [8, 18, 66, 67], we encourage future studies to use the proposed $TP_{e,bi}$ calculation in the evaluation and comparison of 3D steering performance, and to use insights provided in our work to assess the effective throughput calculation in more complex 3D steering applications. Such work can help further validate our proposed calculation, demonstrate its applicability, and support the broader use in 3D steering interactions.

Finally, we observed asymmetric trajectory distributions, e.g., elliptic distribution, shifted in-depth spreads, or boundary-skewed trajectories that deviate from normal distribution assumptions. We suggest that future research explore alternative extensions of the Steering law to treat different axes of the movement separately with different weights in modeling, e.g., [68, 142]. Although we observed no significant learning or fatigue effects across repetition blocks, we emphasize taking such effects into account in future work, particularly in more complicated steering tasks or timely mid-air interactions [57].

7 Conclusion

In this paper, we explore effective throughput, a widely studied performance metric in Human–Computer Interaction (HCI), in 3D steering tasks. To predict linear 3D steering motions, we propose a novel calculation of effective throughput ($TP_{e,bi}$) derived from the bivariate standard deviation of the trajectory as effective width ($W_{e,bi}$) and the total steered distance as effective amplitude (A_e). We recommend that researchers and practitioners adopt these effective parameters in effective throughput calculations, a choice that we empirically support in this work. Our results show that the proposed parameters better capture actual user behavior in 3D mid-air steering, yield more accurate Steering law model-fits, and reduce throughput instability caused by implicit speed–accuracy tradeoffs, thereby supporting a fairer basis for comparative performance evaluation. By providing detailed analyses of both performance and trajectory distributions, our work offers the first step toward understanding effective parameters for 3D steering and establishes a foundation for future research.

Acknowledgments

We greatly thank the reviewers for their insightful and constructive comments. This research was supported by the Natural Sciences and Engineering Research Council of Canada (NSERC) Discovery Grant.

References

[1] Diar Abdlkarim, Massimiliano Di Luca, Poppy Aves, Mohamed Maaroufi, Sang-Hoon Yeo, R Chris Miall, Peter Holland, and Joseph M Galea. 2024. A Methodological Framework to Assess the Accuracy of Virtual Reality Hand-Tracking Systems: A Case Study With the Meta Quest 2. *Behavior research methods* 56, 2 (2024), 1052–1063. doi:10.3758/s13428-022-02051-8

[2] Johnny Accot and Shumin Zhai. 1997. Beyond Fitts' Law: Models for Trajectory-Based HCI Tasks. In *Proceedings of the ACM SIGCHI Conference on Human Factors in Computing Systems*. 295–302. doi:10.1145/258549.258760

[3] Johnny Accot and Shumin Zhai. 1999. Performance Evaluation of Input Devices in Trajectory-Based Tasks: An Application of the Steering Law. In *Proceedings of the SIGCHI conference on Human Factors in Computing Systems*. 466–472. doi:10.1145/302979.303133

[4] Johnny Accot and Shumin Zhai. 2001. Scale Effects in Steering Law Tasks. In *Proceedings of the SIGCHI conference on Human factors in computing systems*. 1–8. doi:10.1145/365024.365027

[5] David Ahlström. 2005. Modeling and Improving Selection in Cascading Pull-Down Menus Using Fitts' Law, the Steering Law and Force Fields. In *Proceedings of the SIGCHI conference on Human factors in computing systems*. 61–70. doi:10.1145/1054972.1054982

[6] David Ahlström, Andy Cockburn, Carl Gutwin, and Pourang Irani. 2010. Why It's Quick to Be Square: Modelling New and Existing Hierarchical Menu Designs. In *Proceedings of the SIGCHI Conference on Human Factors in Computing Systems*. 1371–1380. doi:10.1145/1753326.1753534

[7] Sunyoung Ahn, Sangyeon Kim, and Sangwon Lee. 2021. Effects of Visual Cues on Distance Perception in Virtual Environments Based on Object Identification and Visually Guided Action. *International Journal of Human–Computer Interaction* 37, 1 (2021), 36–46. doi:10.1080/10447318.2020.1805875

[8] Mohammadreza Amini, Wolfgang Stuerzlinger, Robert J Teather, and Anil Ufuk Batmaz. 2025. A Systematic Review of Fitts' Law in 3D Extended Reality. In *Proceedings of the CHI Conference on Human Factors in Computing Systems (CHI '25)*. doi:10.1145/3706598.3713623

[9] Mohammadreza Amini, Wolfgang Stuerzlinger, Shota Yamanaka, Hai-Ning Liang, and Anil Ufuk Batmaz. 2025. Tunnels vs. Wires: A Comparative Analysis of Two 3D Steering Tasks in Virtual Environments. In *31st Symposium on Virtual Reality Software and Technology (VRST '25)*. ACM. doi:10.1145/3756884.3766023

[10] Mohsen Annabestani, Sandhya Sriram, S Chiu Wong, Alexandros Sigaras, and Bobak Mosadegh. 2024. Advanced XR-Based 6-DOF Catheter Tracking System for Immersive Cardiac Intervention Training. *arXiv preprint arXiv:2411.02611* (2024). doi:10.48550/arXiv.2411.02611

[11] Georg Apitz and François Guimbretière. 2004. Crossy: A Crossing-Based Drawing Application. In *Proceedings of the 17th annual ACM symposium on User interface software and technology*. 3–12. doi:10.1145/1029632.1029635

[12] Venkata Arikatla, Sam Horvath, Yaoyu Fu, Lora Cavuoto, Suvranu De, Steve Schwaitzberg, and Andinet Enquobahrie. 2019. Development and Face Validation of a Virtual Camera Navigation Task Trainer. *Surgical endoscopy* 33, 6 (2019), 1927–1937. doi:10.1007/s00464-018-6476-6

[13] Nancy A Baker, Heather Livengood, Amy C Nau, Grace Owens, April J Chambers, Jenna Trout, and Rakié Cham. 2017. Effects of Central and Peripheral Vision Occlusion on Motor Performance During Hand Coordination Tasks. *IISE Transactions on Occupational Ergonomics and Human Factors* 5, 3-4 (2017), 148–157. doi:10.1080/24725838.2017.1398691

[14] Mayra Donaji Barrera Machuca and Wolfgang Stuerzlinger. 2018. Do Stereo Display Deficiencies Affect 3D Pointing?. In *Extended abstracts of the 2018 CHI conference on human factors in computing systems*. 1–6. doi:10.1145/3170427.3188540

[15] Anil Ufuk Batmaz, Mayra Donaji Barrera Machuca, Junwei Sun, and Wolfgang Stuerzlinger. 2022. The Effect of the Vergence-Accommodation Conflict on Virtual Hand Pointing in Immersive Displays. In *Proceedings of the 2022 CHI Conference on Human Factors in Computing Systems*. 1–15. doi:10.1145/3491102.3502067

[16] Anil Ufuk Batmaz, Mayra Donaji Barrera Machuca, Duc Minh Pham, and Wolfgang Stuerzlinger. 2019. Do Head-Mounted Display Stereo Deficiencies Affect 3D Pointing Tasks in AR and VR?. In *2019 IEEE conference on virtual reality and 3D user interfaces (VR)*. IEEE, 585–592. doi:10.1109/VR.2019.8797975

[17] Anil Ufuk Batmaz, Moaaz Hudhud Mughribi, Mine Sarac, Mayra Barrera Machuca, and Wolfgang Stuerzlinger. 2023. Measuring the Effect of Stereo Deficiencies on Peripersonal Space Pointing. In *2023 IEEE conference virtual reality and 3D user interfaces (VR)*. IEEE, 1–11. doi:10.1109/VR55154.2023.00063

[18] Anil Ufuk Batmaz and Wolfgang Stuerzlinger. 2022. Effective Throughput Analysis of Different Task Execution Strategies for Mid-Air Fitts' Tasks in Virtual Reality. *IEEE Transactions on Visualization and Computer Graphics* 28, 11 (2022), 3939–3947. doi:10.1109/TVCG.2022.3203105

[19] Anil Ufuk Batmaz and Wolfgang Stuerzlinger. 2023. Rotational and Positional Jitter in Virtual Reality Interaction in Everyday VR. In *Everyday Virtual and Augmented Reality*. Springer, 89–118. doi:10.1007/978-3-031-05804-2_4

[20] Anil Ufuk Batmaz, Xintian Sun, Dogu Taskiran, and Wolfgang Stuerzlinger. 2019. Hitting the Wall: Mid-Air Interaction for Eye-Hand Coordination. In *Proceedings of the 25th ACM Symposium on Virtual Reality Software and Technology*. 1–5. doi:10.1145/3359996.3364249

[21] Anil Ufuk Batmaz, Rumeysa Turkmen, Mine Sarac, Mayra Donaji Barrera Machuca, and Wolfgang Stuerzlinger. 2023. Re-Investigating the Effect of the Vergence-Accommodation Conflict on 3D Pointing. In *Proceedings of the 29th ACM symposium on virtual reality software and technology*. 1–10. doi:10.1145/3611659.3615686

[22] Doug A Bowman, Donald B Johnson, and Larry F Hodges. 1999. Testbed Evaluation of Virtual Environment Interaction Techniques. In *Proceedings of the ACM symposium on Virtual reality software and technology*. 26–33. doi:10.1145/323663.323667

[23] Gerd Bruder, Frank Steinicke, and Wolfgang Stürzlinger. 2013. Effects of Visual Conflicts on 3D Selection Task Performance in Stereoscopic Display Environments. In *2013 IEEE Symposium on 3D User Interfaces (3DUI)*. IEEE, 115–118. doi:10.1109/3DUI.2013.6550207

[24] Pinaki Chakraborty and Savita Yadav. 2023. Applicability of Fitts' Law to Interaction With Touchscreen: Review of Experimental Results. *Theoretical Issues in Ergonomics Science* 24, 5 (2023), 532–546. doi:10.1080/1463922X.2022.2114034

[25] Jennie J.Y. Chen and Sidney S. Fels. 2025. Curves Ahead: Enhancing the Steering Law for Complex Curved Trajectories. In *Proceedings of the CHI Conference on Human Factors in Computing Systems (CHI '25)*. ACM. doi:10.1145/3706598.3713102

[26] Chris G Christou, Despina Michael-Grigoriou, Dimitris Sokratous, and Marianna Tsiakoulia. 2018. BuzzwireVR: An Immersive Game to Supplement Fine-Motor Movement Therapy. In *ICAT-EGVE*. 149–156. doi:10.2312/egve.20181327

[27] E. R. F. W. Crossman. 1953. The Speed and Accuracy of Simple Hand Movements. *Ergonomics* 2, 3 (1953), 195–204.

[28] Jian Cui and Alexei Sourin. 2018. Mid-Air Interaction With Optical Tracking for 3D Modeling. *Computers & Graphics* 74 (2018), 1–11. doi:10.1016/j.cag.2018.04.004

[29] R. Dachselt and A. Hübner. 2006. A Survey and Taxonomy of 3D Menu Techniques. In *Proceedings of the 12th Eurographics Conference on Virtual Environments* (Lisbon, Portugal) *(EGVE'06)*. Eurographics Association, Goslar, DEU, 89–99. doi:10.5555/2386021.2386035

[30] Raimund Dachselt and Anett Hübner. 2007. Three-Dimensional Menus: A Survey and Taxonomy. *Computers & Graphics* 31, 1 (2007), 53–65. doi:10.1016/j.cag.2006.09.006

[31] Matthew M. Davis, Joseph L. Gabbard, Doug A. Bowman, and Dennis Gracanin. 2016. Depth-Based 3D Gesture Multi-Level Radial Menu for Virtual Object Manipulation. In *2016 IEEE Virtual Reality (VR)*. 169–170. doi:10.1109/VR.2016.7504707

[32] Leah R Enders, Robert J Smith, Stephen M Gordon, Anthony J Ries, and Jonathan Touryan. 2021. Gaze Behavior During Navigation and Visual Search of an Open-World Virtual Environment. *Frontiers in Psychology* 12 (2021), 681042. doi:10.3389/fpsyg.2021.681042

[33] Brett R Fajen and William H Warren. 2003. Behavioral Dynamics of Steering, Obstable Avoidance, and Route Selection. *Journal of Experimental Psychology: Human Perception and Performance* 29, 2 (2003), 343. doi:10.1037/0096-1523.29.2.343

[34] Franz Faul, Edgar Erdfelder, Albert-Georg Lang, and Axel Buchner. 2007. G* Power 3: A Flexible Statistical Power Analysis Program for the Social, Behavioral, and Biomedical Sciences. *Behavior research methods* 39, 2 (2007), 175–191. doi:10.3758/BF03193146

[35] Vicente Ferrer, Yifan Yang, Alex Perdomo, and John Quarles. 2013. Consider Your Clutter: Perception of Virtual Object Motion in AR. In *2013 IEEE International Symposium on Mixed and Augmented Reality (ISMAR)*. 1–6. doi:10.1109/ISMAR.2013.6671835

[36] Philip W Fink, Patrick S Foo, and William H Warren. 2007. Obstacle Avoidance During Walking in Real and Virtual Environments. *ACM Transactions on Applied Perception (TAP)* 4, 1 (2007), 2–es. doi:10.1145/1227134.1227136

[37] Marius Fischer, Bernhard Fuerst, Sing Chun Lee, Javad Fotouhi, Severine Habert, Simon Weidert, Ekkehard Euler, Greg Osgood, and Nassir Navab. 2016. Preclinical Usability Study of Multiple Augmented Reality Concepts for K-Wire Placement. *International Journal of Computer-Assisted Radiology and Surgery* 11, 6 (2016), 1007–1014. doi:10.1007/s11548-016-1363-x

[38] Paul M Fitts. 1954. The Information Capacity of the Human Motor System in Controlling the Amplitude of Movement. *Journal of Experimental Psychology* 47, 6 (1954), 381. doi:10.1037/0096-3445.121.3.262

[39] Paul M Fitts and James R Peterson. 1964. Information Capacity of Discrete Motor Responses. *Journal of Experimental Psychology* 67, 2 (1964), 103. doi:10.1037/h0045689

[40] Jens Förster, E Tory Higgins, and Amy Taylor Bianco. 2003. Speed/Accuracy Decisions in Task Performance: Built-in Trade-off or Separate Strategic Concerns? *Organizational behavior and human decision processes* 90, 1 (2003), 148–164. doi:10.1016/S0749-5978(02)00509-5

[41] Mucahit Gemici, Vrushank Phadnis, and Anil Ufuk Batmaz. 2025. Before hands disappear: Effect of early warning visual feedback method for hand tracking failures in virtual reality. *PLoS One* 20, 6 (2025), e0323796.

[42] Mucahit Gemici, Wolfgang Stuerzlinger, and Anil Ufuk Batmaz. 2024. Object Speed Control with a Signed Distance Field for Distant Mid-Air Object Manipulation in Virtual Reality. In *2024 IEEE International Symposium on Mixed and Augmented Reality (ISMAR)*. IEEE, 465–474. doi:10.1109/ISMAR62088.2024.00061

[43] Darren George and Paul Mallery. 2019. *IBM SPSS Statistics 26 Step by Step: A Simple Guide and Reference.* Routledge. doi:10.4324/9781032622156

[44] Nicolas Gerig, Johnathan Mayo, Kilian Baur, Frieder Wittmann, Robert Riener, and Peter Wolf. 2018. Missing Depth Cues in Virtual Reality Limit Performance and Quality of Three Dimensional Reaching Movements. *PLoS one* 13, 1 (2018). doi:10.1371/journal.pone.0189275

[45] Tovi Grossman and Ravin Balakrishnan. 2005. A Probabilistic Approach to Modeling Two-Dimensional Pointing. *ACM Transactions on Computer-Human Interaction (TOCHI)* 12, 3 (2005), 435–459. doi:10.1145/1096737.1096741

[46] Jens Grubert, Lukas Witzani, Eyal Ofek, Michel Pahud, Matthias Kranz, and Per Ola Kristensson. 2018. Effects of Hand Representations for Typing in Virtual Reality. In *2018 IEEE Conference on Virtual Reality and 3D User Interfaces (VR)*. IEEE, 151–158. doi:10.1109/VR.2018.8446250

[47] Yves Guiard and Halla B Olafsdottir. 2011. On the Measurement of Movement Difficulty in the Standard Approach to Fitts' Law. *PLoS one* 6, 10 (2011). doi:10.1371/journal.pone.0024389

[48] Yves Guiard and Halla H. Olafsdottir. 2010. What is a Zero-Difficulty Movement? A Scale of Measurement Issue in Fitts' Law Research. (Oct. 2010). https://hal.science/hal-00545567 33 pages.

[49] Yves Guiard and Olivier Rioul. 2015. A Mathematical Description of the Speed/Accuracy Trade-Off of Aimed Movement. In *Proceedings of the 2015 British HCI Conference*. ACM, 91–100. doi:10.1145/2783446.2783574

[50] Hilde Haider and Peter A Frensch. 1999. Information Reduction During Skill Acquisition: The Influence of Task Instruction. *Journal of Experimental Psychology: Applied* 5, 2 (1999), 129. doi:10.1037/1076-898X.5.2.129

[51] Asim Hameed, Sebastian Möller, and Andrew Perkis. 2023. How Good Are Virtual Hands? Influences of Input Modality on Motor Tasks in Virtual Reality. *Journal of Environmental Psychology* 92 (2023), 102137. doi:10.1016/j.jenvp.2023.102137

[52] Jeffrey T Hansberger, Chao Peng, Shannon L Mathis, Vaidyanath Areyur Shanthakumar, Sarah C Meacham, Lizhou Cao, and Victoria R Blakely. 2017. Dispelling the Gorilla Arm Syndrome: The Viability of Prolonged Gesture Interactions. In *Virtual, Augmented and Mixed Reality: 9th International Conference, VAMR 2017, Held as Part of HCI International 2017, Vancouver, BC, Canada, July 9-14, 2017, Proceedings 9*. Springer, 505–520. doi:10.1007/978-3-319-57987-0_41

[53] Jakob Hartbrich, Stephanie Arevalo Arboleda, Steve Goring, and Alexander Raake. 2025. The Effect of Hand Visibility in AR: Comparing Dexterity and Interaction with Virtual and Real Objects. *IEEE Transactions on Visualization & Computer Graphics* 31, 11 (Nov. 2025), 10026–10034. doi:10.1109/TVCG.2025.3616868

[54] Amal Hatira, Zeynep Ecem Gelmez, Anil Ufuk Batmaz, and Mine Sarac. 2024. Effect of Hand and Object Visibility in Navigational Tasks Based on Rotational and Translational Movements in Virtual Reality. In *2024 IEEE Conference Virtual Reality and 3D User Interfaces (VR)*. IEEE, 115–125. doi:10.1109/VR58804.2024.00035

[55] Nour Hatira and Mine Sarac. 2025. Fine Motor Tasks in Virtual Reality: The Impact of Haptic Feedback and Object Characterization. *IEEE Access* (2025). doi:10.1109/ACCESS.2025.3581787

[56] Robert F Hess, Long To, Jiawei Zhou, Guangyu Wang, and Jeremy R Cooperstock. 2015. Stereo Vision: The Haves and Have-Nots. *i-Perception* 6, 3 (2015), 2041669515593028. doi:10.1177/2041669515593028

[57] Juan David Hincapié-Ramos, Xiang Guo, Paymahn Moghadasian, and Pourang Irani. 2014. Consumed Endurance: A Metric to Quantify Arm Fatigue of Mid-Air Interactions. In *Proceedings of the SIGCHI conference on human factors in computing systems*. 1063–1072. doi:10.1145/2556288.2557130

[58] David M. Hoffman, Ahna R. Girshick, Kurt Akeley, and Martin S. Banks. 2008. Vergence–Accommodation Conflicts Hinder Visual Performance and Cause Visual Fatigue. *Journal of Vision* 8, 3 (2008), 1–30. doi:10.1167/8.3.33

[59] Errol R Hoffmann. 2009. Review of Models for Restricted-Path Movements. *International Journal of Industrial Ergonomics* 39, 4 (2009), 578–589. doi:10.1016/j.ergon.2008.02.007

[60] Xuning Hu, Xinan Yan, Yushi Wei, Wenxuan Xu, Yue Li, Yue Liu, and Hai-Ning Liang. 2024. Exploring the Effects of Spatial Constraints and Curvature for 3D Piloting in Virtual Environments. In *2024 IEEE International Symposium on Mixed and Augmented Reality (ISMAR)*. IEEE, 505–514. doi:10.1109/ISMAR62088.2024.00065

[61] BSEN ISO and BRITISH STANDARD. 2010. Ergonomics of Human-System Interaction. *British Standards Institution* (2010). webstore.ansi.org/standards/bsi/BSENISO92413042008

[62] Sujin Jang, Wolfgang Stuerzlinger, Satyajit Ambike, and Karthik Ramani. 2017. Modeling Cumulative Arm Fatigue in Mid-Air Interaction Based on Perceived Exertion and Kinetics of Arm Motion. In *Proceedings of the 2017 CHI conference on human factors in computing systems*. 3328–3339. doi:10.1145/3025453.3025523

[63] Alan Jones. 2018. *Best Fit Lines & Curves: And Some Mathe-Magical Transformations.* Routledge. doi:10.4324/9781315160085

[64] J Adam Jones, J Edward Swan, Gurjot Singh, Eric Kolstad, and Stephen R Ellis. 2008. The Effects of Virtual Reality, Augmented Reality, and Motion Parallax on Egocentric Depth Perception. In *Proceedings of the 5th symposium on Applied perception in graphics and visualization*. 9–14. doi:10.1145/1394281.1394283

[65] Jari Kangas, Sriram Kishore Kumar, Helena Mehtonen, Jorma Järnstedt, and Roope Raisamo. 2022. Trade-off Between Task Accuracy, Task Completion Time and Naturalness for Direct Object Manipulation in Virtual Reality. *Multimodal Technologies and Interaction* 6, 1 (2022), 6. doi:10.3390/mti6010006

[66] Nobuhito Kasahara, Yosuke Oba, Shota Yamanaka, Anil Ufuk Batmaz, Wolfgang Stuerzlinger, and Homei Miyashita. 2024. Better Definition and Calculation of Throughput and Effective Parameters for Steering to Account for Subjective Speed-accuracy Tradeoffs. In *Proceedings of the 2024 CHI Conference on Human Factors in Computing Systems*. 1–18. doi:10.1145/3613904.3642084

[67] Nobuhito Kasahara, Yosuke Oba, Shota Yamanaka, Wolfgang Stuerzlinger, and Homei Miyashita. 2023. Throughput and Effective Parameters in Crossing. In *Extended Abstracts of the 2023 CHI Conference on Human Factors in Computing Systems*. 1–9. doi:10.1145/3544549.3585817

[68] Raghavendra S. Kattinakere, Tovi Grossman, and Sriram Subramanian. 2007. Modeling Steering Within Above-The-Surface Interaction Layers. In *Proceedings of the SIGCHI Conference on Human Factors in Computing Systems* (San Jose, California, USA) *(CHI '07)*. Association for Computing Machinery, New York, NY, USA, 317–326. doi:10.1145/1240624.1240678

[69] Nikolaos Katzakis, Lihan Chen, Oscar Ariza, Robert J Teather, and Frank Steinicke. 2019. Evaluation of 3D Pointing Accuracy in the Fovea and Periphery in Immersive Head-Mounted Display Environments. *IEEE Transactions on Visualization and Computer Graphics* 27, 3 (2019), 1929–1936. doi:10.1109/TVCG.2019.2947504

[70] Steven W Keele. 1968. Movement Control in Skilled Motor Performance. *Psychological bulletin* 70, 6p1 (1968), 387. doi:10.1037/h0026739

[71] Youngwon Ryan Kim, Hyeonah Choi, Minwook Chang, and Gerard J. Kim. 2020. Applying Touchscreen Based Navigation Techniques to Mobile Virtual Reality with Open Clip-On Lenses. *Electronics* 9, 9 (2020). doi:10.3390/electronics9091448

[72] Paul B Kline and Bob G Witmer. 1996. Distance Perception in Virtual Environments: Effects of Field of View and Surface Texture at Near Distances. In *Proceedings of the Human Factors and Ergonomics Society annual meeting*, Vol. 40. SAGE Publications Sage CA: Los Angeles, CA, 1112–1116. doi:10.1177/154193129604002201

[73] MH Korayem and V Vahidifar. 2022. Detecting Hand's Tremor Using Leap Motion Controller in Guiding Surgical Robot Arms and Laparoscopic Scissors. *Measurement* 204 (2022), 112133. doi:10.1016/j.measurement.2022.112133

[74] Panagiotis Kourtesis, Sebastian Vizcay, Maud Marchal, Claudio Pacchierotti, and Ferran Argelaguet. 2022. Action-Specific Perception & Performance on a Fitts's Law Task in Virtual Reality: The Role of Haptic Feedback. *IEEE Transactions on Visualization and Computer Graphics* 28, 11 (2022), 3715–3726. doi:10.1109/TVCG.2022.3203003

[75] Joseph J LaViola Jr, Ernst Kruijff, Ryan P McMahan, Doug Bowman, and Ivan P Poupyrev. 2017. *3D User Interfaces: Theory and Practice*. Addison-Wesley Professional, USA.

[76] Khanh-Duy Le, Tanh Quang Tran, Karol Chlasta, Krzysztof Krejtz, Morten Fjeld, and Andreas Kunz. 2021. Vxslate: Exploring Combination of Head Movements and Mobile Touch for Large Virtual Display Interaction. In *Proceedings of the 2021 ACM Designing Interactive Systems Conference*. 283–297. doi:10.1145/3461778.3462076

[77] Zhipeng Li, Yikai Cui, Tianze Zhou, Yu Jiang, Yuntao Wang, Yukang Yan, Michael Nebeling, and Yuanchun Shi. 2022. Color-To-Depth Mappings as Depth Cues in Virtual Reality. In *Proceedings of the 35th annual ACM symposium on user interface software and technology*. 1–14. doi:10.1145/3526113.3545646

[78] Lei Liu, Jean-Bernard Martens, and Robert Van Liere. 2011. Revisiting Path Steering for 3D Manipulation Tasks. *International Journal of Human-Computer Studies* 69, 3 (2011), 170–181. doi:10.1016/j.ijhcs.2010.11.006

[79] Lei Liu and Robert van Liere. 2011. Modeling Object Pursuit for 3D Interactive Tasks in Virtual Reality. In *2011 IEEE Virtual Reality Conference*. IEEE, 3–10. doi:10.1109/VR.2011.5759416

[80] Lei Liu and Robert Van Liere. 2012. Modeling Object Pursuit for Desktop Virtual Reality. *IEEE Transactions on Visualization and Computer Graphics* 18, 7 (2012), 1017–1026. doi:10.1109/TVCG.2012.31

[81] R Duncan Luce. 1991. *Response Times: Their Role in Inferring Elementary Mental Organization*. Oxford University Press. doi:10.1093/acprof:oso/9780195070019.001.0001

[82] Tiffany Luong, Yi Fei Cheng, Max Möbus, Andreas Fender, and Christian Holz. 2023. Controllers or Bare Hands? A Controlled Evaluation of Input Techniques on Interaction Performance and Exertion in Virtual Reality. *IEEE Transactions on Visualization and Computer Graphics* 29, 11 (2023), 4633–4643. doi:10.1109/TVCG.2023.3320211

[83] Donald G MacKay. 1982. The Problems of Flexibility, Fluency, and Speed–Accuracy Trade-off in Skilled Behavior. *Psychological review* 89, 5 (1982), 483. doi:10.1037/0033-295X.89.5.483

[84] I Scott MacKenzie. 1992. Fitts' Law as a Research and Design Tool in Human-Computer Interaction. *Human-computer interaction* 7, 1 (1992), 91–139. doi:10.1207/s15327051hci0701_3

[85] I Scott MacKenzie. 2018. Fitts' Law. *The Wiley Handbook of Human-Computer Interaction* 1 (2018), 347–370. doi:10.1002/9781118976005.ch17

[86] I. Scott MacKenzie and William A. S. Buxton. 1992. Extending Fitts' Law to Two-Dimensional Tasks. In *Proceedings of the SIGCHI Conference on Human Factors in Computing Systems*. ACM, 219–226. doi:10.1145/142750.142794

[87] I Scott MacKenzie and Poika Isokoski. 2008. Fitts' Throughput and the Speed-Accuracy Tradeoff. In *Proceedings of the SIGCHI Conference on Human Factors in Computing Systems*. 1633–1636. doi:10.1145/1357054.1357308

[88] I. Scott MacKenzie and Shumin Zhang. 1999. The Design and Evaluation of a High-Performance Soft Keyboard. In *Proceedings of the SIGCHI Conference on Human Factors in Computing Systems*. 25–31. doi:10.1145/302979.302983

[89] David E. Meyer, J. E. Keith Smith, and Charles E. Wright. 1982. Models for the Speed and Accuracy of Aimed Movements. *Psychological Review* 89, 5 (1982), 449–482. doi:10.1037/0033-295x.89.5.449

[90] Pedro Monteiro, Diana Carvalho, Miguel Melo, Frederico Branco, and Maximino Bessa. 2017. Evaluation of Virtual Reality Navigation Interfaces Using the Steering Law. In *2017 24º Encontro Português de Computação Gráfica e Interação (EPCGI)*. IEEE, 1–7. doi:10.1109/EPCGI.2017.8124299

[91] Pedro Monteiro, Diana Carvalho, Miguel Melo, Frederico Branco, and Maximino Bessa. 2018. Application of the Steering Law to Virtual Reality Walking Navigation Interfaces. *Computers & Graphics* 77 (2018), 80–87. doi:10.1016/j.cag.2018.10.003

[92] Fariba Mostajeran, Moritz Friedrich, Frank Steinicke, Simone Kühn, and Wolfgang Stuerzlinger. 2025. The Effects of Biophilic Design on Steering Performance in Virtual Reality. *Scientific Reports* 15, 1 (2025), 32485. doi:10.1038/s41598-025-19113-4

[93] Yorie Nakahira, Quanying Liu, Terrence J. Sejnowski, and John C. Doyle. 2019. Fitts' Law for Speed-Accuracy Trade-Off Describes a Diversity-Enabled Sweet Spot in Sensorimotor Control. *arXiv preprint arXiv:1906.00905* (2019). https://arxiv.org/abs/1906.00905

[94] Thomas E Nygren. 1997. Framing of Task Performance Strategies: Effects on Performance in a Multiattribute Dynamic Decision Making Environment. *Human Factors* 39, 3 (1997), 425–437. doi:10.1518/001872097778827115

[95] Halla H Olafsdottir, Yves Guiard, Olivier Rioul, and Simon T Perrault. 2012. A New Test of Throughput Invariance in Fitts' Law: Role of the Intercept and of Jensen's Inequality. *Interfaces, the quarterly magazine of BCS interaction group* 93 (2012), 8–pages. doi:10.5555/2377916.2377930

[96] Matheus M Pacheco, Charley W Lafe, and Karl M Newell. 2019. Search Strategies in the Perceptual-Motor Workspace and the Acquisition of Coordination, Control, and Skill. *Frontiers in Psychology* 10 (2019), 1874. doi:10.3389/fpsyg.2019.01874

[97] Robert Pastel. 2006. Measuring the Difficulty of Steering Through Corners. In *Proceedings of the SIGCHI conference on Human Factors in computing systems*. 1087–1096. doi:10.1145/1124772.1124934

[98] Alexandra A Portnova-Fahreeva, Momona Yamagami, Adrià Robert-Gonzalez, Jennifer Mankoff, Heather Feldner, and Katherine M Steele. 2024. Accuracy of Video-Based Hand Tracking for People With Upper-Body Disabilities. *IEEE Transactions on Neural Systems and Rehabilitation Engineering* 32 (2024), 1863–1872. doi:10.1109/TNSRE.2024.3398610

[99] Ivan Poupyrev, Mark Billinghurst, Suzanne Weghorst, and Tadao Ichikawa. 1996. The Go-Go Interaction Technique: Non-Linear Mapping for Direct Manipulation in VR. In *Proceedings of the ACM symposium on User Interface Software and Technology (UIST)*. 79–80. doi:10.1145/237091.237102

[100] Nathaniel V Powell, Xavier Marshall, Gabriel J Diaz, and Brett R Fajen. 2024. Coordination of Gaze and Action During High-Speed Steering and Obstacle Avoidance. *PLoS one* 19, 3 (2024), e0289855. doi:10.3389/fpsyg.2021.681042

[101] Eric D Ragan, Doug A Bowman, Regis Kopper, Cheryl Stinson, Siroberto Scerbo, and Ryan P McMahan. 2015. Effects of Field of View and Visual Complexity on Virtual Reality Training Effectiveness for a Visual Scanning Task. *IEEE Transactions on Visualization and Computer Graphics* 21, 7 (2015), 794–807. doi:10.1109/TVCG.2015.2403312

[102] Vijay Rajanna and Tracy Hammond. 2018. A Fitts' Law Evaluation of Gaze Input on Large Displays Compared to Touch and Mouse Inputs. In *Proceedings of the Workshop on Communication by Gaze Interaction* (Warsaw, Poland) *(COGAIN '18)*. Association for Computing Machinery, New York, NY, USA, Article 8, 5 pages. doi:10.1145/3206343.3206348

[103] Dennis Reimer, Iana Podkosova, Daniel Scherzer, and Hannes Kaufmann. 2023. Evaluation and Improvement of Hmd-Based and Rgb-Based Hand Tracking Solutions in VR. *Frontiers in Virtual Reality* 4 (2023), 1169313. doi:10.3389/frvir.2023.1169313

[104] Xiangshi Ren and Xiaolei Zhou. 2011. An Investigation of the Usability of the Stylus Pen for Various Age Groups on Personal Digital Assistants. *Behaviour & Information Technology* 30, 6 (2011), 709–726. doi:10.1080/01449290903205437

[105] James M Ritchie, Graham Robinson, Philip N Day, Richard G Dewar, Raymond CW Sung, and John EL Simmons. 2007. Cable Harness Design, Assembly and Installation Planning Using Immersive Virtual Reality. *Virtual Reality* 11, 4 (2007), 261–273. doi:10.1007/s10055-007-0073-7

[106] Maria Francesca Roig-Maimó, Ramon Mas-Sansó, and I Scott MacKenzie. 2025. Tracing: The Forgotten Task of ISO 9241. In *Adjunct Proceedings of the 27th International Conference on Mobile Human-Computer Interaction*. 1–7. doi:10.1145/3737821.3749558

[107] Vianney Rozand, Florent Lebon, Charalambos Papaxanthis, and Romuald Lepers. 2015. Effect of Mental Fatigue on Speed–Accuracy Trade-off. *Neuroscience* 297 (2015), 219–230. doi:10.1016/j.neuroscience.2015.03.066

[108] I Scott MacKenzie. 2015. Fitts' Throughput and the Remarkable Case of Touch-Based Target Selection. In *International conference on human-computer interaction*. Springer, 238–249. doi:10.1007/978-3-319-20916-6_23

[109] Ather Sharif, Victoria Pao, Katharina Reinecke, and Jacob O Wobbrock. 2020. The Reliability of Fitts's Law as a Movement Model for People With and Without Limited Fine Motor Function. In *Proceedings of the 22nd international Acm Sigaccess conference on computers and accessibility*. 1–15. doi:10.1145/3373625.3416999

[110] Yilei Shi, Moritz Alexander Messerschmidt, Haimo Zhang, Yuting Chen, and Kaixing Zhao. 2024. UbiPen: Digitizing Analogue Pens with a Finger-Mounted IMU. In *2024 IEEE Smart World Congress (SWC)*. IEEE, 361–368. doi:10.1109/SWC62898.2024.00082

[111] R William Soukoreff and I Scott MacKenzie. 2004. Towards a Standard for Pointing Device Evaluation, Perspectives on 27 Years of Fitts' Law Research in Hci. *International Journal of Human-Computer tudies* 61, 6 (2004), 751–789. doi:10.1016/j.ijhcs.2004.09.001

[112] Howard W Stoudt. 1973. Arm Lengths and Arm Reaches: Some Interrelationships of Structural and Functional Body Dimensions. *American Journal of Physical Anthropology* 38, 1 (1973), 151–161. doi:10.1002/ajpa.1330380129

[113] Ahmed N Sulaiman and Patrick Olivier. 2008. Attribute Gates. In *Proceedings of the 21st annual ACM symposium on User interface software and technology*. 57–66. doi:10.1145/1449715.1449726

[114] Minghui Sun, Xiangshi Ren, and Xiang Cao. 2010. Effects of Multimodal Error Feedback on Human Performance in Steering Tasks. *Journal of Information Processing* 18 (2010), 284–292. doi:10.2197/ipsjjip.18.284

[115] BG Tabachnick and LS Fidell. 2013. Using Multivariate Statistics (6e éd.). Boston, É. *U.: Pearson* (2013).

[116] Robert J Teather, Daniel Natapov, and Michael Jenkin. 2010. Evaluating Haptic Feedback in Virtual Environments Using Iso 9241–9. In *2010 IEEE Virtual Reality Conference (VR)*. IEEE, 307–308. doi:10.1109/VR.2010.5444753

[117] Robert J. Teather and Wolfgang Stuerzlinger. 2011. Pointing at 3D Targets in a Stereo Head-Tracked Virtual Environment. In *2011 IEEE Symposium on 3D User Interfaces (3DUI)*. 87–94. doi:10.1109/3DUI.2011.5759222

[118] Eleftherios Triantafyllidis and Zhibin Li. 2021. The Challenges in Modeling Human Performance in 3D Space With Fitts' Law. In *Extended Abstracts of the 2021 CHI Conference on Human Factors in Computing Systems*. 1–9. doi:10.1145/3411763.3443442

[119] Ryosuke Tsumura and Hiroyasu Iwata. 2017. Trajectory Planning for Abdominal Fine Needle Insertion Based on Insertion Angles. *IEEE Robotics and Automation Letters* 2, 2 (2017), 1226–1231. doi:10.1109/LRA.2017.2670145

[120] Huawei Tu, Susu Huang, Jiabin Yuan, Xiangshi Ren, and Feng Tian. 2019. Crossing-Based Selection With Virtual Reality Head-Mounted Displays. In *Proceedings of the 2019 CHI conference on human factors in computing systems*. 1–14. doi:10.1145/3290605.3300848

[121] Rumeysa Turkmen, Laurent Voisard, Marta Kerten-Oertel, and Anil Ufuk Batmaz. 2025. Adaptive Hand Visibility for Accurate 3D User Interactions in Virtual Environments. In *2025 IEEE International Symposium on Mixed and Augmented Reality (ISMAR*. doi:10.1109/ISMAR67309.2025.00015

[122] Pier Paolo Valentini. 2011. Interactive Cable Harnessing in Augmented Reality. *International Journal on Interactive Design and Manufacturing (IJIDeM)* 5, 1 (2011), 45–53. doi:10.1007/s12008-010-0114-4

[123] Sarah Van Der Land, Alexander P Schouten, Frans Feldberg, Bart van Den Hooff, and Marleen Huysman. 2013. Lost in Space? Cognitive Fit and Cognitive Load in 3D Virtual Environments. *Computers in Human Behavior* 29, 3 (2013), 1054–1064. doi:10.1016/j.chb.2012.09.006

[124] Ana Maria Villanueva, Sujin Jang, Wolfgang Stuerzlinger, Satyajit Ambike, and Karthik Ramani. 2023. Advanced Modeling Method for Quantifying Cumulative Subjective Fatigue in Mid-Air Interaction. *International Journal of Human-Computer Studies* 169, Article 102931 (Jan 2023), 15 pages. doi:10.1016/j.ijhcs.2022.102931

[125] Laurent Voisard, Amal Hatira, Mine Sarac, Marta Kersten-Oertel, and Anil Ufuk Batmaz. 2023. Effects of Opaque, Transparent and Invisible Hand Visualization Styles on Motor Dexterity in a Virtual Reality Based Purdue Pegboard Test. In *2023 IEEE International Symposium on Mixed and Augmented Reality (ISMAR)*. 723–731. doi:10.1109/ISMAR59233.2023.00087

[126] Tim Wächter and Matthias König. 2024. Indoor Drone Path Planning with Real/Virtual Obstacles by Mixed Reality. In *2024 IEEE International Symposium on Mixed and Augmented Reality Adjunct (ISMAR-Adjunct)*. IEEE, 600–603. doi:10.1109/ISMAR-Adjunct64951.2024.00172

[127] Uta Wagner, Mathias N Lystbæk, Pavel Manakhov, Jens Emil Sloth Grønbæk, Ken Pfeuffer, and Hans Gellersen. 2023. A Fitts' Law Study of Gaze-Hand Alignment for Selection in 3D User Interfaces. In *Proceedings of the 2023 CHI Conference on Human Factors in Computing Systems*. 1–15. doi:10.1145/3544548.3581423

[128] Yushi Wei, Rongkai Shi, Anil Ufuk Batmaz, Yue Li, Mengjie Huang, Rui Yang, and Hai-Ning Liang. 2024. Evaluating and Modeling the Effect of Frame Rate on Steering Performance in Virtual Reality. *IEEE Transactions on Visualization and Computer Graphics* (2024). doi:10.1109/TVCG.2024.3451491

[129] Yushi Wei, Kemu Xu, Yue Li, Lingyun Yu, and Hai-Ning Liang. 2024. Exploring and Modeling Directional Effects on Steering Behavior in Virtual Reality. *IEEE Transactions on Visualization and Computer Graphics* (2024). doi:10.1109/TVCG.2024.3456166

[130] Jannik Wiese and Niels Henze. 2023. Predicting Mouse Positions Beyond a System's Latency Can Increase Throughput and User Experience in Linear Steering Tasks. In *Proceedings of Mensch und Computer 2023*. ACM, 101–115. doi:10.1145/3603555.3603556

[131] Jacob O Wobbrock and Krzysztof Z Gajos. 2007. A Comparison of Area Pointing and Goal Crossing for People With and Without Motor Impairments. In *Proceedings of the 9th international ACM SIGACCESS conference on Computers and accessibility*. 3–10. doi:10.1145/1296843.1296847

[132] Jacob O. Wobbrock, Kristen Shinohara, and Alex Jansen. 2011. The Effects of Task Dimensionality, Endpoint Deviation, Throughput Calculation, and Experiment Design on Pointing Measures and Models. In *Proceedings of the SIGCHI Conference on Human Factors in Computing Systems* (Vancouver, BC, Canada) *(CHI '11)*. Association for Computing Machinery, New York, NY, USA, 1639–1648. doi:10.1145/1978942.1979181

[133] Shota Yamanaka. 2022. Test-Retest Reliability on Movement Times and Error Rates in Target Pointing. In *Proceedings of the 2022 ACM Designing Interactive Systems Conference*. 178–188. doi:doi.org/10.1145/3532106.3533450

[134] Shota Yamanaka, Taiki Kinoshita, Yosuke Oba, Ryuto Tomihari, and Homei Miyashita. 2023. Varying Subjective Speed-Accuracy Biases to Evaluate the Generalizability of Experimental Conclusions on Pointing-Facilitation Techniques. In *Proceedings of the 2023 CHI Conference on Human Factors in Computing Systems*. 1–13. doi:10.1145/3544548.3580740

[135] Shota Yamanaka and Homei Miyashita. 2016. Modeling the Steering Time Difference Between Narrowing and Widening Tunnels. In *Proceedings of the 2016 CHI conference on human factors in computing systems*. 1846–1856. doi:10.1145/2858036.2858037

[136] Shota Yamanaka and Homei Miyashita. 2019. Modeling Pen Steering Performance in a Single Constant-Width Curved Path. In *Proceedings of the 2019 ACM international conference on interactive surfaces and spaces*. 65–76. doi:10.1145/3343055.3359697

[137] Shota Yamanaka and Wolfgang Stuerzlinger. 2020. Necessary and Unnecessary Distractor Avoidance Movements Affect User Behaviors in Crossing Operations. *ACM Transactions on Computer-Human Interaction (TOCHI)* 27, 6 (2020), 1–31. doi:10.1145/3418413

[138] Shota Yamanaka and Wolfgang Stuerzlinger. 2024. The Effect of Latency on Movement Time in Path-steering. In *Proceedings of the 2024 CHI Conference on Human Factors in Computing Systems*. 1–19. doi:10.1145/3613904.3642316

[139] Shota Yamanaka, Wolfgang Stuerzlinger, and Homei Miyashita. 2017. Steering Through Sequential Linear Path Segments. In *Proceedings of the 2017 CHI conference on human factors in computing systems*. 232–243. doi:10.1145/3025453.3025836

[140] Shota Yamanaka, Wolfgang Stuerzlinger, and Homei Miyashita. 2018. Steering Through Successive Objects. In *Proceedings of the 2018 CHI conference on human factors in computing systems*. 1–13. doi:10.1145/3173574.3174177

[141] Shota Yamanaka, Takumi Takaku, Yukina Funazaki, Noboru Seto, and Satoshi Nakamura. 2023. Evaluating the Applicability of GUI-Based Steering Laws to VR Car Driving: A Case of Curved Constrained Paths. *Proceedings of the ACM on Human-Computer Interaction* 7, ISS (2023), 93–113. doi:10.1145/3626466

[142] Shota Yamanaka, Hiroki Usuba, and Homei Miyashita. 2022. Bivariate Effective Width Method to Improve the Normalization Capability for Subjective Speed-Accuracy Biases in Rectangular-Target Pointing. In *Proceedings of the 2022 CHI conference on human factors in computing systems*. 1–13. doi:10.1145/3491102.3517466

[143] Shota Yamanaka, Hiroki Usuba, Yosuke Oba, Taiki Kinoshita, Ryuto Tomihari, Nobuhito Kasahara, and Homei Miyashita. 2024. Verifying Finger-Fitts Models for Normalizing Subjective Speed-Accuracy Biases. *Proceedings of the ACM on Human-Computer Interaction* 8, MHCI (2024), 1–24. doi:10.1145/3676532

[144] Ai-ping Yang, Hui-min Hu, Xin Zhang, Li Ding, and Chau-Kuang Chen. 2021. Natural and Forced Arm Reach Ranges in Sitting Position. *International Journal of Industrial Ergonomics* 86 (2021), 103185. doi:10.1016/j.ergon.2021.103185

[145] Mona Zavichi, André Santos, Catarina Moreira, Anderson Maciel, and Joaquim Jorge. 2025. Gaze-Hand Steering for Travel and Multitasking in Virtual Environments. arXiv:2504.01906 [cs.HC] https://arxiv.org/abs/2504.01906

[146] Shumin Zhai. 2004. Characterizing Computer Input With Fitts' Law Parameters—The Information and Non-Information Aspects of Pointing. *International Journal of Human-Computer Studies* 61, 6 (2004), 791–809. doi:10.1016/j.ijhcs.2004.09.006

[147] Shumin Zhai, Johnny Accot, and Rogier Woltjer. 2004. Human Action Laws in Electronic Virtual Worlds: An Empirical Study of Path Steering Performance in VR. *Presence* 13, 2 (2004), 113–127. doi:10.1162/1054746041382393

[148] Shumin Zhai, Jing Kong, and Xiangshi Ren. 2004. Speed–Accuracy Tradeoff in Fitts' Law Tasks—On the Equivalency of Actual and Nominal Pointing Precision. *International Journal of Human-Computer Studies* 61, 6 (2004), 823–856. doi:10.1016/j.ijhcs.2004.09.007

[149] Hang Zhao, Kaiyan Ling, IV Ramakrishnan, MD Guy Schwartz, and Xiaojun Bi. 2025. Modeling Mouse-based Pointing and Steering Tasks for People with Parkinson's Disease. *Proceedings of the ACM on Interactive, Mobile, Wearable and Ubiquitous Technologies* 9, 1 (2025), 1–24. doi:10.1145/3712267

[150] Yuxin Zhao and Zuen Cen. 2024. Exploring Multimodal Feedback Mechanisms for Improving User Interaction in Virtual Reality Environments. *Journal of Industrial Engineering and Applied Science* 2, 6 (2024), 35–41. doi:10.70393/6a69656173.323331

[151] Xiaolei Zhou, Shengdong Zhao, Mark Chignell, and Xiangshi Ren. 2011. Assessing Age-Related Performance Decrements in User Interface Tasks. In *2011 IEEE International Conference on Information and Automation*. IEEE, 817–822. doi:10.1109/ICINFA.2011.5949107

[152] Antonio Zorcolo, Enrico Gobbetti, Gianluigi Zanetti, and Massimiliano Tuveri. 2000. A Volumetric Virtual Environment for Catheter Insertion Simulation. In *Virtual Environments 2000*, Jurriaan Mulder and Robert van Liere (Eds.). Springer Vienna, 125–134. doi:10.1007/978-3-7091-6785-4_14